

罗迪尼亞大陸西北緣俯衝作用:來自藏北安多拉伸紀花崗片麻岩的證據

楊寧,胡培遠*,翟慶國,唐躍,劉一鳴,李金勇

中國地質科學院地質研究所,北京,100037

內容摘要:羅迪尼亞超大陸的古地理重建和各陸塊拼接方案一直是中外地球科學家關注和競相研究的熱點和前沿。目前,青藏高原各陸塊的起源及其在羅迪尼亞超大陸中的古地理位置尚不清楚,岩漿事件的對比研究是解決這一問題的有效方法之一。本文報道了青藏高原中部安多微陸塊的拉伸紀花崗片麻岩的LA-ICP-MS鑽石U-Pb定年、岩石地球化學和鑽石Hf和全岩Sr-Nd同位素分析結果。這些花崗片麻岩的原岩形成於802~801 Ma,具有不均一的鑽石Hf和相對均一的全岩Nd同位素成分($\epsilon_{\text{Hf}}(t) = -9.4 \sim +1.9$; $\epsilon_{\text{Nd}}(t) = -4.8 \sim -3.4$)以及古老的地殼模式年齡(2289~1575 Ma),可能形成於幔源岩漿對元古宙地殼的改造,隨後經歷了廣泛的結晶分異過程。花崗片麻岩樣品具有較低的 P_2O_5 含量, P_2O_5 與 SiO_2 含量呈負相關性,且含少量角閃石礦物,符合I型花崗岩的特徵,其中部分樣品具有較高的高場強元素含量($Zr + Ce + Nb + Y > 350 \times 10^{-6}$)和鑽石飽和溫度(>800°C),因而兼具A型花崗岩的特徵。綜合前人研究成果與區域地質背景,中國安多地區拉伸紀花崗片麻岩可能形成於弧後盆地環境,與馬達加斯加、塞舌爾和印度西部的同時代岩漿記錄可以對比,從而為重建羅迪尼亞超大陸提供了新的依據。

關鍵詞:青藏高原;安多微陸塊;全岩地球化學;鑽石U-Pb定年

超大陸的聚合和裂解是地球演化最基本的規律之一(Zhao Guochun et al., 2018)。通過研究超大陸,不仅可以探索地球早期形成、演化過程與動力學機制,還可以為有關礦產的形成與分布提供約束。羅迪尼亞是一個中—新元古代的超大陸,於1.1~0.9 Ga前拼合而成,750~600 Ma左右完全解體(Torsvik, 2003; Goodge et al., 2008; Li Zhengxiang et al., 2008; Zheng Yongfei et al., 2008a, 2008b)。近年來,羅迪尼亞超大陸的古地理重建和各陸塊拼接方案一直是中外地球科學家關注和競相研究的熱點和前沿(Dalziel, 1991; Hoffman, 1991; Moores, 1991; Torsvik, 2003; Goodge et al., 2008; Li Zhengxiang et al., 2008)。拉伸紀(1000~720 Ma)是羅迪尼亞超大陸演化的關鍵時期,代表了該超大陸的初始裂解階段。在這

一時期,全球不同成因的岩漿事件存在相對有序的時空分布,主要表現為超大陸內部的岩石圈伸展和超大陸邊緣的洋-陸俯衝過程(Collins and Pisarevsky, 2005; Cawood et al., 2017),因而岩漿事件的對比研究可以為陸塊的古地理位置提供約束。

青藏高原位於阿爾卑斯-喜馬拉雅巨型特提斯造山帶的東段,是地球上最年輕和最高的高原(Yin An and Harrison, 2000; Zhai Qingguo et al., 2013, 2016)。隨著近年來地質研究程度的提高,青藏高原古生代—中生代的板塊構造演化過程已經日趨清晰(Yin An and Harrison, 2000; 莫宣學等, 2005; 潘桂棠等, 2006; Zhu Dicheng et al., 2009a, 2009b, 2010, 2011, 2012, 2013; Yang Tiannan et al., 2011, 2014),但是對於青藏高原各

注:本文為國家自然科學基金項目(編號42072268, 41872240)、第二次青藏高原綜合科學考察項目(編號2019QZKK0703)、國家重點研發計劃(編號2021YFC2901901)、中國地質科學院地質研究所基本科研業務經費(編號J2202)和中國地質調查項目(編號20221630)聯合資助的成果。

收稿日期:2022-06-14;改回日期:2022-08-18;網絡發表日期:2022-11-04;責任編委:張招崇;責任編輯:蔡志慧。

作者簡介:楊寧,男,1998年生。碩士生,構造地質學專業。E-mail: 198346227@qq.com。

* 通訊作者:胡培遠,男,1987年生。博士,研究員,從事青藏高原早期形成與演化研究。E-mail: azure_jlu@126.com。

引用本文:楊寧,胡培遠,翟慶國,唐躍,劉一鳴,李金勇. 2023. 羅迪尼亞大陸西北緣俯衝作用:來自藏北安多拉伸紀花崗片麻岩的證據. 地質學報, 97(6): 1797~1814, doi: 10.19762/j.cnki.dizhixuebao.2022183.

Yang Ning, Hu Peiyuan, Zhai Qingguo, Tang Yue, Liu Yiming, Li Jinyong. 2023. Oceanic subduction along the northwestern margin of the Rodinia: Evidence from the Tonian granite gneisses in the Amdo area, northern Tibet. Acta Geologica Sinica, 97(6): 1797~1814.

陆块前寒武纪演化历史的认知程度仍然很低,各陆块在罗迪尼亞超大陆中的古地理位置仍不清楚。在青藏高原中—新生代的强烈构造运动过程中,大量的前寒武纪基底岩石被抬升、剥蚀,从而出露于地表。青藏高原上的拉伸纪岩石主要分布于拉萨地块和安多微陆块。前人已经对拉萨地块上的拉伸纪岩浆事件开展了较为系统的研究。与此对应的是,安多微陆块上虽然报道了多处拉伸纪岩浆岩,但是研究程度较低,前人研究多处于野外描述和定年研究阶段,缺少系统的岩石成因和构造背景研究,制约了对安多微陆块古地理亲缘性的探索。针对这一问题,本文以安多微陆块内拉伸纪花岗片麻岩为研究对象,对其进行详细的岩石学、锆石 U-Pb 年龄、全岩地球化学以及 Sr-Nd-Hf 同位素研究。在此基础上,探讨其岩石成因和构造背景,进而约束安多微陆块的前寒武纪演化过程及其在罗迪尼亞超大陆重建中的古地理位置。

1 地质背景

青藏高原是一个巨大的构造拼合体,其由多个地块或微地块、多条蛇绿混杂岩带以及多条造山带体系所组成(Yin An and Harrison, 2000)。青藏高原大地构造格架划分出五条主缝合带,从北向南依次为:康西瓦-玛沁-昆仑山缝合带、西金乌兰-金沙

江缝合带、龙木错-双湖-澜沧江缝合带、班公湖-怒江缝合带和印度河-雅鲁藏布江缝合带。这些缝合带所划分的地块依次为巴颜喀拉-甘孜地块、羌北-昌都地块、羌南-保山地块、拉萨地块和喜马拉雅地块(图 1a)。班公湖-怒江缝合带是青藏高原上一条重要的构造分界线,主要由蛇绿岩、洋岛、复理石岩片和微陆块等组成。安多微陆块是东西走向的巨大眼球状地体,其两侧均保留有班公湖-怒江洋残留的蛇绿混杂岩。

青藏高原最具代表性的新元古代基底岩石为拉萨地块中—西部的念青唐古拉岩群和安多微陆块上的安多片麻岩。念青唐古拉岩群由李璞等(1955)所称的念青唐古拉片麻岩和那更拉片岩系演变而来,主要岩石类型为斜长角闪岩、花岗片麻岩、白云母石英片岩、石英岩等。早期的相关研究工作主要聚焦于念青唐古拉岩群中岩浆和变质事件的年代学研究,获得了 897~660 Ma 的岩浆结晶年龄和 680~650 Ma 的变质年龄(胡道功等, 2005; Dong Xin et al., 2011; Zhang Zeming et al., 2012b)。近年来,国内学者对念青唐古拉岩群开展了较为精细的岩石成因和构造背景研究工作,从中识别出了以下 4 期岩浆-沉积-变质记录:930~902 Ma 裂谷岩浆-沉积记录(Hu Peiyuan et al., 2018c)、822~671 Ma 岛弧岩浆-变质记录(Hu Peiyuan et al., 2018a,

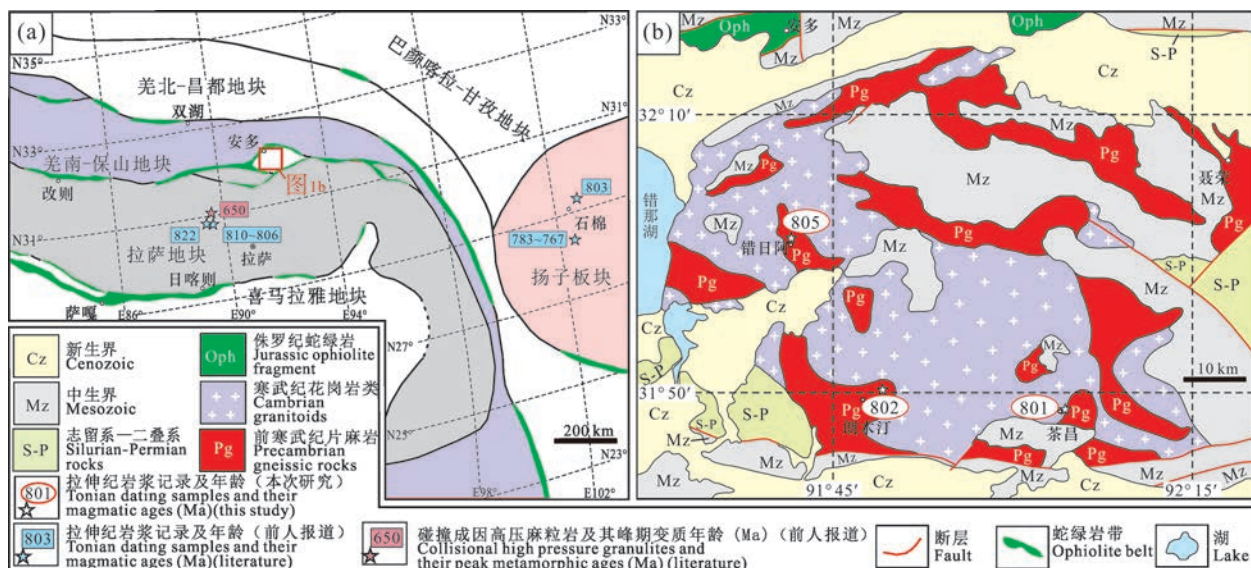


图 1 青藏高原中部构造划分简图(a)和安多地区区域地质简图(b)(据 Hu Peiyuan et al., 2021)

Fig. 1 Simplified tectonic map of the central Tibetan Plateau (a) and geological map of the Amdo area (b)

年龄资料引自 Hu Peiyuan et al., 2018b (822 Ma, 810~806 Ma); Huang Xiaolong et al., 2008 (783~767 Ma); Li Xianhua et al., 2002b (803 Ma); Zhang Zeming et al., 2012b (650 Ma)

The data were quoted from Hu Peiyuan et al., 2018b (822 Ma, 810~806 Ma); Huang Xiaolong et al., 2008 (783~767 Ma); Li Xianhua et al., 2002b (803 Ma); Zhang Zeming et al., 2012b (650 Ma)

2018b; Zhou Xiang et al., 2019)、658~646 Ma 碰撞型岩漿-變質記錄(Zhang Zeming et al., 2012b; Hu Peiyuan et al., 2019a, 2022)和 572~500 Ma 活動大陸邊緣岩漿-沉積記錄(Zhu Dichen et al., 2012; Ding Huixia et al., 2015; Hu Peiyuan et al., 2018d, 2019b, 2021)。安多片麻岩以花崗片麻岩為主,也見少量變質沉積岩和基性岩漿岩(Guynn et al., 2012; Zhang Zeming et al., 2012a)。前人已在安多片麻岩中識別出了拉伸紀花崗質岩漿記錄,獲得的鋯石 U-Pb 年齡為 910~799 Ma(Guynn et al., 2012; Zhang Zeming et al., 2012a; 王明等, 2012; 解超明等, 2014),但是其岩石成因和構造背景尚不清楚。

本次重點研究安多微陸塊上錯日阿、朗木汀和茶昌地區前寒武紀花崗片麻岩的形成時代、岩石成因與構造背景,采樣位置見圖 1b。錯日阿花崗片麻岩岩體(樣品 18T514~519)呈岩株狀產出,與前寒武紀副片麻岩圍岩接觸面不規則,可見明顯侵入接

觸關係(圖 2a)。岩體受後期構造作用及風化影響,多破碎成不同規模的岩塊。正交偏光顯微鏡下樣品呈現中粗粒變晶結構,片麻狀構造,有明顯定向(圖 2b),礦物組成主要為石英(35%~40%)、斜長石(25%~30%)、正長石(25%~30%)、黑雲母(5%~10%)和角閃石(2%~5%)(圖 2c)。石英多呈他形,粒度為 0.5~3.0 mm,波狀消光,發生了顆粒邊界遷移重結晶作用;斜長石多呈板柱狀,自形一半自形,部分發生蝕變現象,粒度為 0.2~1.0 mm,可見聚片雙晶;正長石為肉紅色,自形一半自形,粒度為 0.2~1.0 mm,角閃石呈長柱狀,有兩組近 60°解理,干涉色為一級橙色到二級藍綠色,自形一半自形,粒度為 0.2~0.5 mm,與黑雲母呈共生關係。朗木汀花崗片麻岩岩體(樣品 18T555~557)與茶昌花崗片麻岩岩體(樣品 18T584~589)出露面積較小,岩體與圍岩接觸部位被第四紀地層所覆蓋(圖 2d),正交偏光顯微鏡下均为中粗粒變晶結構,片麻狀構造,有明顯定向(圖 2e)。礦物組成主要為石英(35%~40%)、

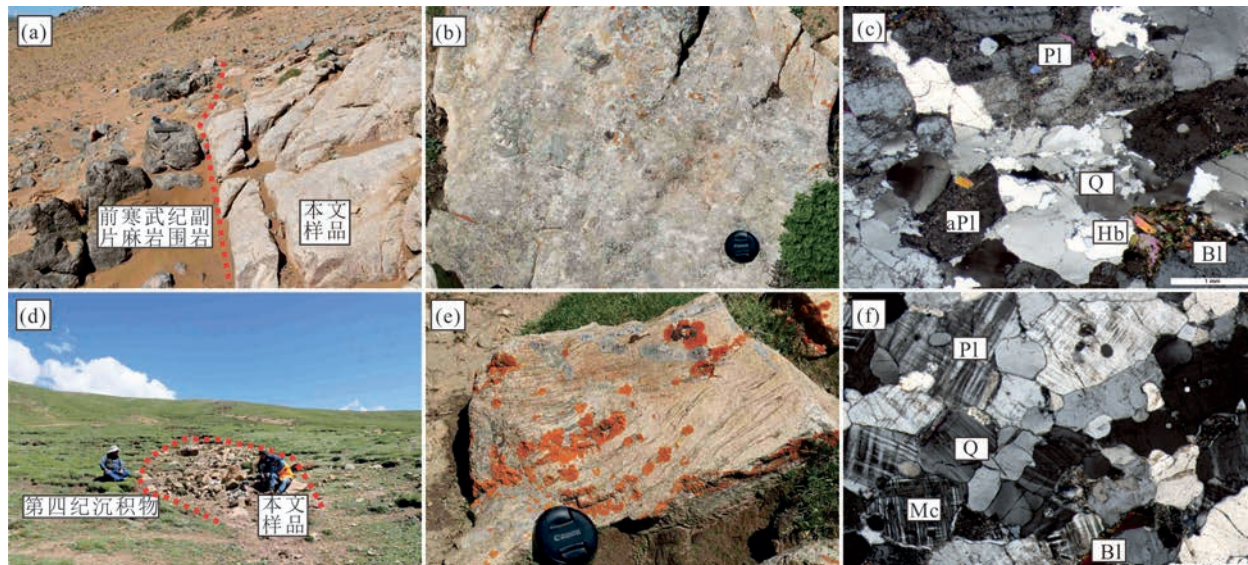


圖 2 安多地區花崗片麻岩的野外露頭照片(a,b,d,e)和顯微鏡正交偏光下照片(c,f)

Fig. 2 Photographs (a, b, d, e) and photomicrographs under crossed polarized light (c, f) of the granitic gneisses in the Amdo area

(a)—錯日阿花崗片麻岩與前寒武紀副片麻岩的侵入接觸界線;(b)—花崗片麻岩的露頭近景照片,顯示受到了後期蝕變的影響;(c)—錯日阿花崗片麻岩顯微鏡正交偏光下照片,部分長石可見蝕變現象;(d)—朗木汀和茶昌花崗片麻岩與圍岩接觸關係被第四紀地層所覆蓋;(e)—朗木汀和茶昌花崗片麻岩的露頭的典型照片,可見明顯片麻狀構造;(f)—朗木汀和茶昌花崗片麻岩的典型顯微鏡正交偏光下照片,礦物有明顯定向;Q—石英;Pl—斜長石;aPl—蝕變斜長石;Bl—黑雲母;Mc—微斜長石;Hb—角閃石

(a)—boundary of the intrusive contact between Cuoria granite gneisses and Precambrian paragneisses; (b)—close-up photograph of an outcrop of granitic gneiss, showing that it has been affected by late alteration; (c)—under orthogonally polarized microscope, some feldspar can be seen alteration in Cuoria granite gneiss; (d)—contact relationship between Langmuting and Chachang granitic gneisses and surrounding rocks is covered by Quaternary strata; (e)—typical photographs of outcrops of Langmuting and Chachang granitic gneiss, showing distinct gneis-like structures; (f)—typical microscopically orthogonally polarized photographs of Langmuting and Chachang granitic gneiss, showing obvious mineral orientation; Q—quartz; Pl—plagioclase; aPl—altered plagioclase; Bl—biotite; Mc—microcline; Hb—hornblende

表 1 安多花岗片麻岩的锆石 LA-ICP-MS U-Pb-Th 分析结果

Table 1 U-Th-Pb isotope compositions of zircons in Amdo granitic gneiss as measured by LA-ICP-MS

测点	元素含量($\times 10^{-6}$)			Th/U	同位素比值						同位素年龄(Ma)					
	Pb _{rad}	²³² Th	²³⁸ U		²⁰⁷ Pb/ ²⁰⁶ Pb	1σ	²⁰⁷ Pb/ ²³⁵ U	1σ	²⁰⁶ Pb/ ²³⁸ U	1σ	²⁰⁷ Pb/ ²⁰⁶ Pb	1σ	²⁰⁷ Pb/ ²³⁵ U	1σ	²⁰⁶ Pb/ ²³⁸ U	1σ
18T514, 32°1'16.471"N, 91°41'36.003"E																
18T514-01	79	460	440	1.05	0.0671	0.0011	1.22	0.0227	0.1322	0.0019	843	34	811	10	800	11
18T514-02	199	933	1196	0.78	0.0674	0.0009	1.23	0.0176	0.1323	0.0014	850	22	814	8	801	8
18T514-03	44	224	261	0.86	0.0695	0.0019	1.27	0.0317	0.1326	0.0021	922	56	831	14	803	12
18T514-04	170	743	1062	0.70	0.0705	0.0019	1.28	0.0390	0.1322	0.0048	943	57	838	17	800	27
18T514-05	65	435	358	1.22	0.0698	0.0015	1.27	0.0348	0.1323	0.0026	922	46	834	16	801	15
18T514-06	34	139	204	0.68	0.0745	0.0033	1.35	0.0554	0.1322	0.0022	1054	91	868	24	800	13
18T514-07	81	457	476	0.96	0.0679	0.0014	1.24	0.0260	0.1322	0.0018	865	37	817	12	800	10
18T514-08	60	407	329	1.24	0.0680	0.0012	1.24	0.0228	0.1322	0.0015	878	37	818	10	800	9
18T514-09	108	788	569	1.39	0.0659	0.0012	1.20	0.0257	0.1323	0.0018	803	39	801	12	801	10
18T514-10	72	439	414	1.06	0.0674	0.0013	1.23	0.0266	0.1322	0.0018	850	45	813	12	800	10
18T514-11	168	1204	902	1.33	0.0682	0.0013	1.24	0.0280	0.1323	0.0021	876	44	820	13	801	12
18T514-12	57	247	345	0.72	0.0680	0.0021	1.24	0.0413	0.1325	0.0026	878	-134	819	19	802	15
18T514-13	50	260	299	0.87	0.0689	0.0016	1.25	0.0293	0.1322	0.0014	894	44	825	13	800	8
18T514-14	101	648	561	1.16	0.0681	0.0013	1.24	0.0269	0.1320	0.0015	872	45	819	12	799	8
18T514-15	66	414	392	1.06	0.0657	0.0019	1.18	0.0359	0.1321	0.0028	798	56	793	17	800	16
18T514-16	36	137	226	0.61	0.0666	0.0013	1.21	0.0237	0.1323	0.0016	833	41	806	11	801	9
18T514-17	49	254	288	0.88	0.0678	0.0013	1.24	0.0232	0.1323	0.0014	865	35	817	11	801	8
18T514-18	77	287	490	0.59	0.0678	0.0012	1.23	0.0238	0.1320	0.0017	865	37	816	11	799	9
18T514-19	26	92	164	0.56	0.0697	0.0020	1.27	0.0366	0.1320	0.0014	920	57	831	16	799	8
18T514-20	226	808	1429	0.57	0.0678	0.0009	1.24	0.0180	0.1322	0.0012	861	28	817	8	800	7
18T514-21	63	222	397	0.56	0.0655	0.0017	1.20	0.0426	0.1320	0.0023	791	55	799	20	799	13
18T514-22	121	386	766	0.50	0.0671	0.0021	1.23	0.0557	0.1323	0.0040	839	64	813	25	801	22
18T514-23	73	452	412	1.10	0.0662	0.0031	1.21	0.0516	0.1327	0.0024	813	92	805	24	803	14
18T554, 31°50'15.926"N, 91°49'50.987"E																
18T554-01	160	165	1018	0.16	0.2620	0.1543	1.72	0.1014	0.1327	0.0216	3259	1104	1015	38	803	123
18T554-02	158	189	415	0.46	0.1134	0.0013	5.24	0.0651	0.3351	0.0035	1855	20	1859	11	1863	17
18T554-03	251	718	621	1.16	0.1008	0.0013	4.22	0.0602	0.3035	0.0030	1639	23	1678	12	1708	15
18T554-04	79	232	528	0.44	0.0714	0.0019	1.30	0.0302	0.1328	0.0019	969	50	847	13	804	11
18T554-05	30	63	828	0.08	0.0504	0.0020	0.25	0.0099	0.0356	0.0004	213	91	225	8	226	3
18T554-06	42	135	299	0.45	0.0661	0.0014	1.20	0.0378	0.1324	0.0039	809	46	800	17	802	22
18T554-07	464	286	1424	0.20	0.1054	0.0010	4.41	0.0751	0.3028	0.0046	1722	17	1713	14	1705	23
18T554-08	94	577	519	1.11	0.0728	0.0027	1.34	0.0802	0.1320	0.0045	1009	75	864	35	799	25
18T554-09	193	218	1097	0.20	0.0729	0.0008	1.70	0.0224	0.1691	0.0015	1013	23	1009	8	1007	8
18T554-10	181	159	1313	0.12	0.0745	0.0012	1.36	0.0235	0.1321	0.0020	1054	33	871	10	800	11
18T554-11	110	171	419	0.41	0.0876	0.0011	2.87	0.0472	0.2379	0.0029	1373	24	1375	12	1376	15
18T554-12	39	55	303	0.18	0.0713	0.0017	1.30	0.1097	0.1315	0.0103	966	48	847	48	796	58
18T554-13	115	199	417	0.48	0.0876	0.0016	2.93	0.0564	0.2426	0.0030	1374	35	1390	15	1400	16
18T554-14	151	80	477	0.17	0.1154	0.0014	4.68	0.0801	0.2942	0.0039	1887	22	1764	14	1662	19
18T554-15	142	375	973	0.39	0.0682	0.0010	1.25	0.0320	0.1327	0.0030	876	24	823	14	803	17
18T554-16	117	539	734	0.73	0.0657	0.0010	1.20	0.0232	0.1324	0.0021	798	31	801	11	802	12
18T554-17	168	1097	960	1.14	0.0672	0.0015	1.23	0.0284	0.1324	0.0024	843	45	812	13	802	14
18T554-18	97	428	389	1.10	0.0766	0.0011	2.03	0.0306	0.1927	0.0021	1109	30	1126	10	1136	12
18T554-19	36	63	1038	0.06	0.0541	0.0012	0.26	0.0080	0.0353	0.0007	372	56	237	6	224	4
18T554-20	44	135	1505	0.09	0.0495	0.0008	0.20	0.0036	0.0296	0.0003	169	39	187	3	188	2
18T554-21	83	327	559	0.59	0.0643	0.0013	1.17	0.0540	0.1322	0.0055	750	44	788	25	800	31
18T554-22	136	668	887	0.75	0.0656	0.0023	1.19	0.0563	0.1320	0.0040	794	81	798	26	799	23
18T584, 31°50'21.359"N, 92°3'20.466"E																
18T584-01	130	575	819	0.70	0.0664	0.0011	1.21	0.0199	0.1322	0.0014	817	34	805	9	800	8
18T584-02	122	497	777	0.64	0.0659	0.0011	1.20	0.0230	0.1324	0.0017	1200	36	802	11	801	10
18T584-03	200	654	1318	0.50	0.0650	0.0013	1.19	0.0259	0.1322	0.0020	776	43	795	12	800	11
18T584-04	44	150	301	0.50	0.0625	0.0013	1.14	0.0336	0.1319	0.0030	692	47	772	16	799	17

续表1

测点	元素含量($\times 10^{-6}$)			Th/U	同位素比值					同位素年龄(Ma)						
	Pb _{rad}	²³² Th	²³⁸ U		²⁰⁷ Pb/ ²⁰⁶ Pb	1 σ	²⁰⁷ Pb/ ²³⁵ U	1 σ	²⁰⁶ Pb/ ²³⁸ U	1 σ	²⁰⁷ Pb/ ²⁰⁶ Pb	1 σ	²⁰⁷ Pb/ ²³⁵ U	1 σ	²⁰⁶ Pb/ ²³⁸ U	1 σ
18T584-05	156	528	1029	0.51	0.0678	0.0017	1.23	0.0262	0.1320	0.0023	863	53	816	12	799	13
18T584-06	93	289	616	0.47	0.0637	0.0016	1.16	0.0252	0.1323	0.0013	731	52	783	12	801	7
18T584-07	91	348	583	0.60	0.0669	0.0020	1.22	0.0314	0.1322	0.0025	835	65	809	14	801	14
18T584-08	105	478	654	0.73	0.0663	0.0010	1.21	0.0191	0.1320	0.0015	817	32	804	9	799	9
18T584-09	75	277	486	0.57	0.0640	0.0012	1.17	0.0268	0.1322	0.0020	743	42	785	13	800	11
18T584-10	58	368	331	1.11	0.0687	0.0020	1.26	0.0574	0.1323	0.0039	900	59	827	26	801	22
18T584-11	161	674	1020	0.66	0.0660	0.0015	1.20	0.0254	0.1321	0.0017	806	44	801	12	800	10
18T584-12	126	566	787	0.72	0.0656	0.0012	1.20	0.0231	0.1323	0.0023	792	38	799	11	801	13
18T584-13	150	684	930	0.74	0.0681	0.0017	1.24	0.0336	0.1320	0.0019	872	50	819	15	799	11
18T584-14	100	738	553	1.34	0.0786	0.0027	1.48	0.1274	0.1321	0.0078	1165	67	923	52	800	44
18T584-15	137	693	821	0.84	0.0671	0.0012	1.22	0.0248	0.1319	0.0028	843	-160	810	11	799	16
18T584-16	221	873	1386	0.63	0.0694	0.0013	1.27	0.0380	0.1326	0.0029	909	37	834	17	803	16
18T584-17	113	374	741	0.50	0.0675	0.0015	1.23	0.0305	0.1323	0.0028	854	48	816	14	801	16
18T584-18	132	541	845	0.64	0.0660	0.0015	1.21	0.0296	0.1325	0.0021	806	44	804	14	802	12
18T584-19	86	389	545	0.71	0.0679	0.0032	1.23	0.0297	0.1321	0.0033	865	98	815	14	800	19
18T584-20	134	484	875	0.55	0.0648	0.0013	1.18	0.0276	0.1323	0.0023	769	43	793	13	801	13
18T584-21	104	594	608	0.98	0.0665	0.0012	1.21	0.0265	0.1320	0.0021	833	36	806	12	799	12
18T584-22	103	390	654	0.60	0.0677	0.0034	1.22	0.0265	0.1323	0.0035	861	106	809	12	801	20
18T584-23	119	455	756	0.60	0.0663	0.0019	1.21	0.0335	0.1326	0.0029	815	60	806	15	803	16

表2 安多花岗片麻岩的锆石Hf同位素组成

Table 2 Hf isotope compositions of zircons from the granitic gneiss in the Amdo area

测点号	年龄(Ma)	同位素比值					¹⁷⁶ Hf/ ¹⁷⁷ Hf _i	$\epsilon_{\text{Hf}}(0)$	$\epsilon_{\text{Hf}}(t)$	2 σ	t_{DM} (Ma)	t_{DMC} (Ma)	$f_{\text{Lu/Hf}}$	
		¹⁷⁶ Yb/ ¹⁷⁷ Hf	1 σ	¹⁷⁶ Lu/ ¹⁷⁷ Hf	1 σ	¹⁷⁶ Hf/ ¹⁷⁷ Hf								
18T514-1	800	0.040668	0.000824	0.001378	0.000024	0.282336	0.000018	0.282315	-15.4	1.5	0.6	1308	1601	-0.96
18T514-2	800	0.032541	0.001099	0.001148	0.000039	0.282306	0.000019	0.282289	-16.5	0.6	0.7	1341	1659	-0.97
18T514-3	800	0.026398	0.000629	0.000949	0.000021	0.282275	0.000016	0.282261	-17.6	-0.4	0.6	1378	1723	-0.97
18T514-5	800	0.063807	0.002689	0.002103	0.000082	0.282283	0.000018	0.282252	-17.3	-0.7	0.6	1409	1742	-0.94
18T514-7	800	0.022272	0.000763	0.000792	0.000025	0.282266	0.000017	0.282254	-17.9	-0.7	0.6	1385	1738	-0.98
18T514-8	800	0.039094	0.000823	0.001385	0.000023	0.282297	0.000019	0.282276	-16.8	0.1	0.7	1363	1689	-0.96
18T514-9	800	0.071097	0.001680	0.002413	0.000052	0.282291	0.000021	0.282254	-17.0	-0.7	0.7	1411	1736	-0.93
18T514-10	800	0.029645	0.000538	0.001059	0.000019	0.282290	0.000019	0.282274	-17.0	0.0	0.7	1361	1693	-0.97
18T514-11	800	0.035467	0.000738	0.001200	0.000022	0.282289	0.000017	0.282271	-17.1	-0.1	0.6	1367	1699	-0.96
18T514-12	800	0.042806	0.000734	0.001508	0.000016	0.282295	0.000022	0.282273	-16.9	0.0	0.8	1370	1696	-0.95
18T514-13	800	0.023733	0.000583	0.000872	0.000019	0.282280	0.000020	0.282267	-17.4	-0.2	0.7	1368	1709	-0.97
18T514-14	800	0.058771	0.001588	0.001960	0.000046	0.282302	0.000020	0.282272	-16.6	0.0	0.7	1377	1697	-0.94
18T514-15	800	0.057584	0.001353	0.002045	0.000046	0.282327	0.000023	0.282297	-15.7	0.8	0.8	1344	1642	-0.94
18T514-16	800	0.029055	0.000292	0.001122	0.000020	0.282344	0.000022	0.282327	-15.1	1.9	0.8	1288	1575	-0.97
18T514-18	800	0.042889	0.000724	0.001507	0.000028	0.282288	0.000024	0.282266	-17.1	-0.3	0.8	1380	1712	-0.95
18T554-4	802	0.025762	0.000146	0.000971	0.000003	0.282316	0.000015	0.282302	-16.1	1.1	0.5	1321	1630	-0.97
18T554-6	802	0.025970	0.000348	0.001024	0.000017	0.282326	0.000021	0.282310	-15.8	1.4	0.7	1310	1611	-0.97
18T554-8	802	0.022690	0.000119	0.000874	0.000004	0.282150	0.000018	0.282137	-22.0	-4.8	0.6	1549	1996	-0.97
18T554-10	802	0.042538	0.000570	0.001476	0.000030	0.282027	0.000018	0.282005	-26.3	-9.4	0.7	1747	2289	-0.96
18T554-12	802	0.019652	0.000834	0.000655	0.000028	0.282047	0.000016	0.282037	-25.6	-8.3	0.6	1682	2218	-0.98
18T554-15	802	0.033683	0.000869	0.001251	0.000042	0.282274	0.000015	0.282255	-17.6	-0.6	0.5	1391	1734	-0.96
18T554-16	802	0.031698	0.000987	0.001231	0.000047	0.282321	0.000017	0.282303	-15.9	1.1	0.6	1323	1627	-0.96
18T554-17	802	0.029228	0.000567	0.000957	0.000016	0.282284	0.000016	0.282270	-17.3	-0.1	0.6	1366	1701	-0.97
18T554-21	802	0.042817	0.000179	0.001408	0.000005	0.282342	0.000016	0.282320	-15.2	1.7	0.6	1301	1588	-0.96
18T554-23	802	0.035858	0.000809	0.001375	0.000025	0.282272	0.000014	0.282251	-17.7	-0.7	0.5	1398	1742	-0.96
18T584-1	801	0.034903	0.000769	0.001149	0.000024	0.282287	0.000016	0.282269	-17.2	-0.1	0.6	1369	1703	-0.97
18T584-2	801	0.041321	0.000701	0.001301	0.000021	0.282332	0.000018	0.282312	-15.6	1.4	0.6	1311	1607	-0.96

续表 2

测点号	年龄 (Ma)	同位素比值					$\epsilon_{\text{Hf}}^{(176\text{Hf}/177\text{Hf})_i}$	$\epsilon_{\text{Hf}}(0)$	$\epsilon_{\text{Hf}}(t)$	2σ	t_{DM} (Ma)	t_{DMC} (Ma)	$f_{\text{Lu/Hf}}$	
		$^{176}\text{Yb}/^{177}\text{Hf}$	1σ	$^{176}\text{Lu}/^{177}\text{Hf}$	1σ	$^{176}\text{Hf}/^{177}\text{Hf}$								
18T584-3	801	0.037825	0.000873	0.001197	0.000026	0.282279	0.000016	0.282261	-17.4	-0.4	0.6	1382	1722	-0.96
18T584-5	801	0.047933	0.000515	0.001585	0.000014	0.282330	0.000019	0.282306	-15.6	1.2	0.7	1323	1621	-0.95
18T584-6	801	0.036249	0.000271	0.001161	0.000007	0.282301	0.000017	0.282283	-16.7	0.4	0.6	1350	1671	-0.97
18T584-7	801	0.038511	0.000629	0.001213	0.000017	0.282303	0.000020	0.282285	-16.6	0.5	0.7	1348	1668	-0.96
18T584-8	801	0.051760	0.000465	0.001700	0.000013	0.282332	0.000016	0.282307	-15.5	1.2	0.6	1324	1619	-0.95
18T584-9	801	0.026312	0.000105	0.000895	0.000003	0.282318	0.000018	0.282305	-16.0	1.2	0.6	1316	1624	-0.97
18T584-11	801	0.062185	0.000638	0.002013	0.000021	0.282309	0.000019	0.282279	-16.4	0.2	0.7	1369	1681	-0.94
18T584-12	801	0.054910	0.000318	0.001805	0.000014	0.282329	0.000019	0.282302	-15.7	1.0	0.7	1333	1631	-0.95
18T584-15	801	0.050590	0.000481	0.001622	0.000014	0.282292	0.000022	0.282267	-17.0	-0.2	0.8	1379	1707	-0.95
18T584-17	801	0.044643	0.001292	0.001484	0.000035	0.282330	0.000022	0.282307	-15.6	1.2	0.8	1320	1618	-0.96
18T584-18	801	0.048569	0.000997	0.001523	0.000022	0.282241	0.000018	0.282218	-18.8	-1.9	0.6	1448	1818	-0.95
18T584-19	801	0.039861	0.000318	0.001273	0.000009	0.282338	0.000021	0.282318	-15.4	1.6	0.8	1302	1593	-0.96
18T584-20	801	0.039869	0.000960	0.001252	0.000021	0.282311	0.000022	0.282292	-16.3	0.7	0.8	1339	1653	-0.96

微斜长石(15%~20%)、斜长石(10%~15%)、正长石(25%~30%)和黑云母(5%~10%)(图 2f)。石英多呈他形,粒度为 0.5~3.0 mm,波状消光;微斜长石多呈板柱状,自形一半自形,粒度为 0.2~1.0 mm,可见格子双晶;斜长石多呈板柱状,自形一半自形,粒度为 0.2~1.0 mm,可见聚片双晶;正长石为肉红色,自形一半自形,粒度为 0.2~1.0 mm。

2 样品测试方法

锆石的分选在河北省区域地质调查院完成,采用常规的重液和磁选方法进行分选,最后在双目显微镜下挑纯。样品靶的制备在中国地质科学院地质研究所完成,制成的样品靶直径为 25 mm。锆石的阴极荧光图像分析在中国地质科学院地质研究所的阴极荧光分析系统(HITACH S-3000N 型场发射环境扫描电镜和 Gatan 公司 Chroma 阴极荧光谱仪)上完成。样品的锆石 U-Pb 测年在北京科荟测试技术有限公司完成,分析仪器为美国 ESI 公司生产的 NWR 193 nm 激光剥蚀进样系统和德国 AnlyitikJena 公司生产的 PQMS Elite 型四级杆等离子体质谱仪联合构成的激光等离子体质谱仪(LA-ICP-MS)。本次分析中激光器工作频率为 10 Hz;测试点束斑直径为 25 μm,剥蚀采样时间为 45 s,具体分析流程见侯可军等(2009)。锆石 GJ-1 (Jackson et al., 2004)作为外部标准来校正分析过程中的同位素分馏,获得的²⁰⁶Pb/²³⁸U 平均年龄为 600.3±7 Ma,与推荐值(599.8±1.7 Ma)在误差范围内保持一致。锆石 U-Pb 年龄用 ICPMSDataCal 数据处理软件(Liu Yongsheng et al., 2010)计算获得,加权平均年龄的计算和谐和图的绘制采用

ISOPLOT 3.0 程序(Ludwig, 2003)。锆石 Hf 同位素分析在中国科学院地质与地球物理研究所 Neptune 多接收电感耦合等离子质谱仪(MC-ICPMS)和 193 nm 激光取样系统上进行,仪器的运行条件及详细的分析过程参见 Wu Fuyuan et al. (2006)。采用单点剥蚀模式,斑束固定为 44 μm。实验测定过程中,MUD 标准锆石的¹⁷⁶Hf / ¹⁷⁷Hf 的测定结果是 0.282505±21,与前人获得的结果一致(Wu Fuyuan et al., 2006)。全岩地球化学样品的主量元素、微量元素、稀土元素以及 Sr-Nd 同位素的分析均在北京科荟测试技术有限公司完成。主量元素采用 X-射线荧光光谱仪(SHIMADZU XRF-1800)分析。微量元素和稀土元素的分析仪器为 Analyticjena PQMS elite 等离子质谱仪,实验室分析详细方法见相关参考文献(Hu Peiyuan et al., 2019a)。选择 3 个典型全岩样品(18T514、18T554、18T584)进行 Sr-Nd 同位素分析,采用的仪器是 Thermo Fisher 公司的型号为 Neptune Plus 的多接收电感耦合等离子体质谱仪(MC-ICP-MS)。

3 分析结果

3.1 锆石 U-Pb 年代学

本文对 3 个样品中的锆石进行了 U-Pb 定年分析,测试结果见表 1。花岗片麻岩样品中的锆石颗粒大部分相似,其长度范围为 50~150 μm,长宽比为 3:1~2:1。大多数锆石为透明、无色、自形颗粒,表现出规则的振荡环带,部分颗粒周围可见窄的浅色变质边(图 3)。依据测点位置、获得的年龄和 Th/U 比值,可将锆石测点分为 3 组。第一组测点的²⁰⁶Pb/²³⁸U 年龄约为 800 Ma,其较高的 Th/U 比

值($0.12\sim1.39$; >0.1)以及岩浆成因振荡环带的存在表明锆石为岩浆成因(吴元保和郑永飞, 2004)。18T514、18T554和18T584样品中的该组锆石测点获得的 $^{206}\text{Pb}/^{238}\text{U}$ 年龄加权平均值分别为 801 ± 4 Ma、 802 ± 10 Ma和 801 ± 5 Ma, 代表了花岗片麻岩原岩的岩浆结晶年龄。第二组锆石年龄明显大于800 Ma ($1863\sim1007$ Ma), 其 $\text{Th}/\text{U}>0.1$ ($0.2\sim1.16$), 位于锆石核部, 应当为古老的继承锆石。第三组锆石年龄明显小于800 Ma ($224\sim673$ Ma), 其 $\text{Th}/\text{U}<0.1$ ($0.06\sim0.09$), 推测其为后期变质年龄。

3.2 锆石 Lu-Hf 和全岩 Sr-Nd 同位素

样品的锆石 Lu-Hf 同位素是在锆石 U-Pb 定年的同一颗锆石的相同部位或相同结构的邻近部位测定的, 测试结果见表 2。样品中锆石的 $^{176}\text{Yb}/^{177}\text{Hf}$

和 $^{176}\text{Lu}/^{177}\text{Hf}$ 比值变化范围分别为 $0.019652\sim0.071097$ 和 $0.000655\sim0.002413$, $^{176}\text{Lu}/^{177}\text{Hf}$ 比值非常接近或小于 0.002, 表明这些锆石形成以后, 基本没有明显的放射性成因 Hf 的积累, 所测定的 $^{176}\text{Hf}/^{177}\text{Hf}$ 比值可以代表其形成锆石时体系的 Hf 同位素组成(吴福元等, 2007)。花岗片麻岩中锆石的 $\epsilon_{\text{Hf}}(t)$ 值介于 $-9.4\sim+1.9$ 之间; 二阶段 Hf 模式年龄(t_{DMC})变化范围为 $1575\sim2289$ Ma, 平均值为 1710 Ma。

3 件全岩样品具有相似的全岩 Sr-Nd 同位素组成, 初始 $^{87}\text{Sr}/^{86}\text{Sr}$ 比值 I_{Sr} 分别为 0.701279、0.698485 和 0.711274, $\epsilon_{\text{Nd}}(t)$ 值介于 $-4.8\sim-2.5$ 之间, 地壳模式年龄介于 $1757\sim1972$ Ma 之间, 与锆石 Hf 地壳模式年龄相当。

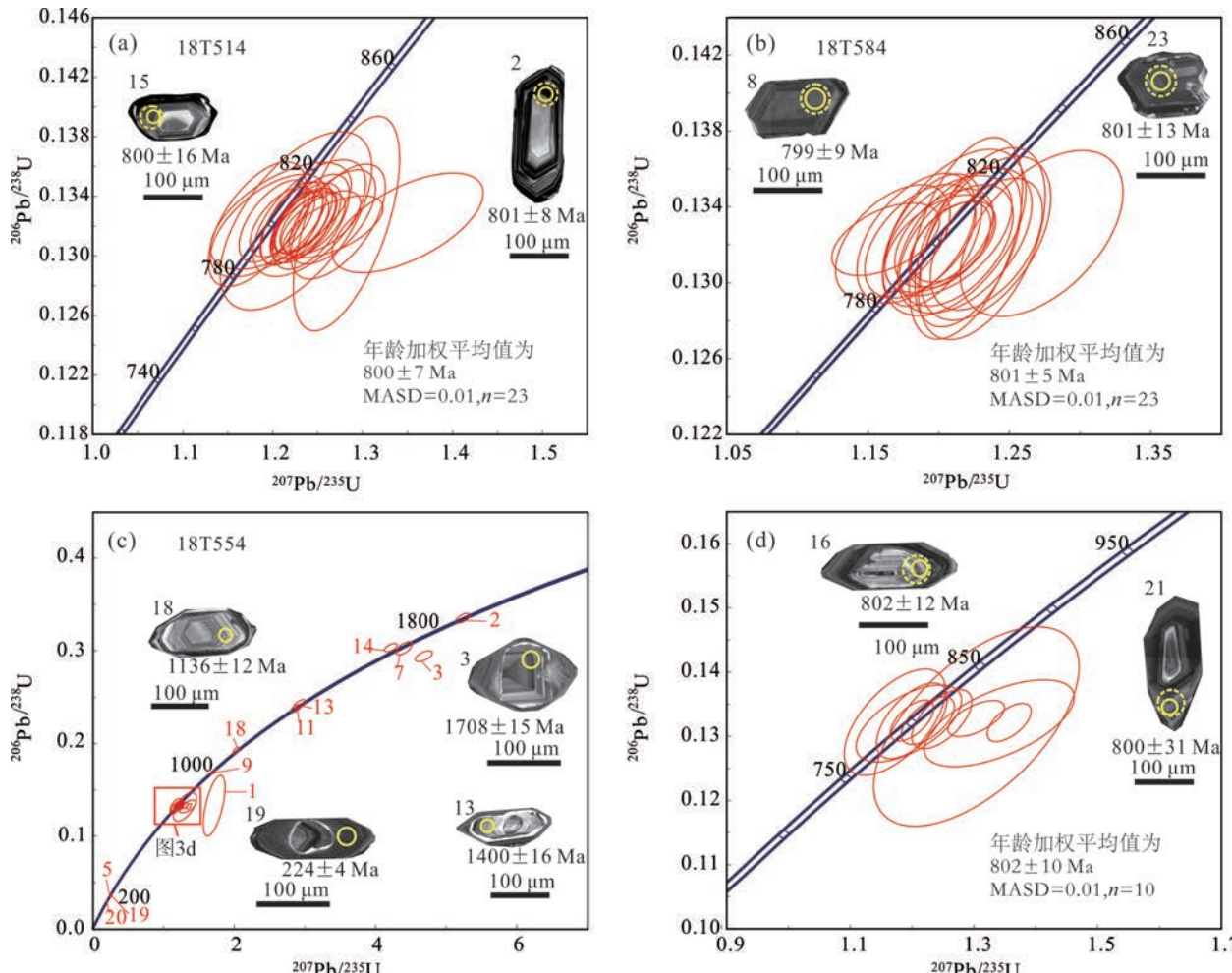


图3 安多花岗片麻岩中典型锆石的阴极荧光图像和锆石的 U-Pb 谱和图

Fig. 3 Cathodoluminescence images of representative zircon grains and U-Pb zircon concordia diagrams of the granitic gneisses in the Amdo area

图中实线圈为锆石 U-Pb 年龄分析点, 虚线圈为锆石 Hf 分析点

The solidcircles are the zircon U-Pb age analysis spots, and the dashed circles are the zircon Hf analysis spots

表 3 安多花岗片麻岩全岩 Sr-Nd 同位素组成

Table 3 Whole-rock Sr-Nd isotopic compositions of the granitic gneiss in the Amdo area

样品号	年龄 (Ma)	Rb ($\times 10^{-6}$)	Sr ($\times 10^{-6}$)	$^{87}\text{Rb}/^{86}\text{Sr}$	$^{87}\text{Sr}/^{86}\text{Sr}$	$\pm 2\sigma$	I_{Sr}	Sm ($\times 10^{-6}$)	Nd ($\times 10^{-6}$)	$^{147}\text{Sm}/^{144}\text{Nd}$	$^{143}\text{Nd}/^{144}\text{Nd}$	$\pm 2\sigma$	$\epsilon_{\text{Nd}}(0)$	$\epsilon_{\text{Nd}}(t)$	$f_{\text{Sm/Nd}}$	t_{DMC} (Ma)
18T514	800	198.73	90.94	6.364	0.774441	0.000005	0.702	2.33	13.1	0.1079	0.512043	0.000004	-11.6	-2.5	-0.45	1757
18T554	801	190.64	161.2	3.432	0.737790	0.000006	0.699	1.09	5.74	0.1148	0.511960	0.000004	-13.2	-4.8	-0.42	1899
18T584	802	140.15	83.98	4.856	0.766826	0.000005	0.711	4.96	34.2	0.0878	0.511892	0.000005	-14.6	-3.4	-0.55	1972

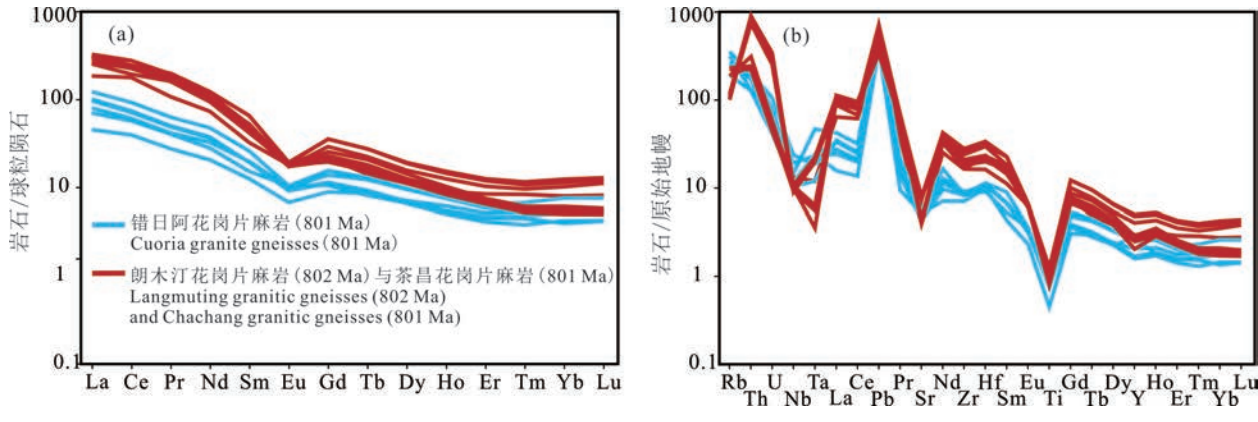


图 4 安多花岗片麻岩的球粒陨石标准化稀土元素配分图(a)和原始地幔标准化微量元素蛛网图(b)(标准化值据 Sun and McDonough, 1989)

Fig. 4 Chondrite-normalized REE (a) and primitive mantle-normalized trace element (b) patterns of the granitic gneiss in the Amdo area (normalization values are after Sun and McDonough, 1989)

3.3 全岩地球化学

花岗片麻岩样品的主量元素和微量元素的分析结果见表 4。将主量元素测试结果扣除烧失量作归一化处理后, 样品含 SiO_2 73.61%~77.04% (为高硅特征), Al_2O_3 12.11%~14.33%, TiO_2 0.13%~0.30%, TFe_2O_3 1.24%~2.40%。在哈克图解上, Al_2O_3 、 TiO_2 、 TFe_2O_3 、 MgO 、 P_2O_5 和 Zr 均与 SiO_2 呈现负相关关系(图 8)。在球粒陨石标准化的稀土元素模式图上, 所有样品的曲线一致性较好, 均表现为右倾的海鸥型, 同时具有明显负 Eu 异常(图 4a)。在原始地幔标准化的微量元素蛛网图上, 样品亏损 Nb、Ta、Sr、Y 和 Ti 元素, 富集 Th、Pb 等元素(图 4b)。值得注意的是, 相对于错日阿花岗片麻岩 (18T514-519; $\text{Zr} + \text{Ce} + \text{Nb} + \text{Y} = 121 \times 10^{-6} \sim 174 \times 10^{-6}$; $T_{\text{zr}} = 731 \sim 747^\circ\text{C}$), 朗木汀花岗片麻岩 (18T555-557; $\text{Zr} + \text{Ce} + \text{Nb} + \text{Y} = 411 \times 10^{-6} \sim 491 \times 10^{-6}$; $T_{\text{zr}} = 836 \sim 849^\circ\text{C}$) 与茶昌花岗片麻岩 (18T584-589; $\text{Zr} + \text{Ce} + \text{Nb} + \text{Y} = 315 \times 10^{-6} \sim 424 \times 10^{-6}$; $T_{\text{zr}} = 786 \sim 818^\circ\text{C}$) 具有较高的高场强元素含量和锆石饱和温度(T_{zr})。

4 讨论

4.1 变质和蚀变作用对元素成分的影响

在变质和蚀变作用过程中, 高场强元素和稀土

元素是相对不活动的, 而大离子亲石元素是易活动元素 (Verma, 1981; Hart and Staudigel, 1982; Zhang Zhaochong et al., 2012)。由于安多花岗片麻岩经历了后期的变质作用改造, 因此在利用全岩地球化学数据讨论其岩石成因和构造环境之前需探讨元素的活动性。为了评估变质作用和蚀变对活动元素组成的影响, 本文选择典型的活动元素(Na、K、Ca 和 Rb)、过渡元素(Mg 和 Fe)和不活动元素(Zr、Th 和 Y)与 LOI(烧失量)进行投图(部分元素的含量由其氧化物的含量代替)。结果显示, 部分活动元素受到蚀变影响而表现出与 LOI 的线性关系(例如: Rb), 不活动元素和过渡元素都没有受到影响(图 5)。因此, 本次研究主要依据过渡元素和不活动元素的含量来对样品进行岩石学分类和成因讨论。

4.2 岩石成因

花岗片麻岩样品具有变化的锆石 $\epsilon_{\text{Hf}}(t)$ 值 ($-9.4 \sim +1.9$) 和较为恒定的全岩 $\epsilon_{\text{Nd}}(t)$ 值 ($-4.8 \sim -3.4$)。这种同位素组成有两种可能解释。① 样品具有均一的岩浆源区, Hf 同位素成分差异是地壳深熔作用过程中不同高场强元素富集矿物参与熔融比例不同的结果。② 样品具有不均一的岩浆源区, 其成因可能与壳-幔混合相关; 锆石封闭温度较

表4 安多花岗片麻岩的全岩主量元素(%)和微量元素($\times 10^{-6}$)分析结果Table 4 Whole-rock major (%) and trace element ($\times 10^{-6}$) data of the granitic gneiss in the Amdo area

样品号	18T514	18T515	18T516	18T517	18T518	18T519	18T555	18T556	18T557	18T584	18T585	18T586	18T587	18T588	18T589
SiO ₂	74.71	75.42	74.89	74.72	74.75	76.00	75.34	73.61	75.04	76.82	76.62	76.15	76.73	77.04	75.48
TiO ₂	0.19	0.20	0.19	0.21	0.20	0.13	0.26	0.30	0.28	0.17	0.22	0.20	0.18	0.22	0.22
Al ₂ O ₃	13.51	13.23	13.55	13.65	13.47	13.12	13.79	14.33	13.64	12.39	12.34	12.58	12.39	12.12	12.11
TFe ₂ O ₃	1.64	1.66	1.59	1.47	1.81	1.24	1.97	2.40	2.36	1.45	1.75	1.61	1.44	1.71	1.69
MnO	0.04	0.04	0.04	0.05	0.05	0.03	0.03	0.03	0.03	0.03	0.02	0.02	0.03	0.03	0.03
MgO	0.50	0.43	0.42	0.52	0.47	0.43	0.37	0.43	0.41	0.25	0.28	0.25	0.24	0.31	0.29
CaO	1.68	1.72	1.67	1.75	1.69	1.21	2.83	2.95	2.88	1.14	1.20	1.23	1.10	1.35	1.42
Na ₂ O	3.32	3.68	3.68	3.15	3.66	4.11	4.02	4.18	4.11	2.81	2.65	2.74	2.74	2.87	2.87
K ₂ O	4.14	3.70	3.99	4.64	3.95	3.45	1.36	1.46	1.09	4.63	4.84	4.89	5.01	4.01	3.93
P ₂ O ₅	0.05	0.04	0.04	0.06	0.04	0.03	0.04	0.05	0.04	0.03	0.03	0.03	0.02	0.03	0.03
LOI	0.42	0.61	0.81	0.56	0.77	0.93	0.81	0.77	0.86	0.73	0.98	0.83	0.71	0.92	0.89
Total	100.20	100.74	100.87	100.77	100.85	100.68	100.82	100.49	100.75	100.45	100.93	100.55	100.59	100.61	98.95
Ti	1080.62	1088.22	977.92	1112.50	1085.50	589.09	1358.31	1639.46	1470.70	1054.52	1338.70	1250.61	1050.80	1301.14	1329.04
Li	8.26	7.46	7.40	9.86	7.59	5.63	13.90	15.41	14.28	11.17	11.62	12.65	12.53	16.12	18.67
Be	2.70	3.20	3.39	3.09	3.59	3.14	4.49	4.81	4.68	1.37	1.20	1.36	1.20	1.40	1.60
Sc	6.73	4.15	4.11	4.16	4.68	2.94	3.28	3.83	3.54	5.65	4.40	4.10	3.72	4.56	4.31
V	23.90	23.63	22.75	21.19	22.15	17.15	27.62	34.60	33.02	14.63	9.15	7.93	6.49	8.30	7.34
Co	3.33	2.01	1.84	2.63	2.02	1.60	2.68	3.21	3.10	2.54	1.72	1.55	1.47	2.04	1.93
Ni	7.25	3.54	3.98	8.11	3.50	6.60	5.93	5.60	5.53	5.82	2.19	1.36	3.38	4.21	4.21
Cu	5.34	5.42	6.26	11.37	6.31	3.44	3.91	3.31	3.69	11.75	7.58	6.31	6.01	11.22	8.63
Zn	32.20	28.13	25.71	31.84	29.45	14.60	26.91	29.86	28.25	19.79	28.13	27.02	24.32	22.01	24.57
Ga	13.08	14.69	14.80	14.51	16.17	13.16	17.16	18.78	18.22	11.96	15.08	14.93	14.27	14.66	15.35
Rb	198.73	151.42	161.60	224.41	167.47	121.05	67.80	73.57	63.63	140.15	141.22	140.24	146.38	118.98	118.39
Sr	90.94	105.02	106.30	98.92	117.90	109.23	160.70	166.41	154.53	83.98	89.92	92.02	86.30	88.75	91.33
Zr	92.79	101.42	91.52	99.19	94.49	79.04	267.13	313.35	281.99	182.98	213.50	203.82	189.16	234.68	233.61
Nb	13.75	7.39	8.43	16.76	10.49	8.10	6.44	7.63	6.99	9.50	7.74	7.09	6.54	7.11	7.45
Ta	0.94	0.49	0.96	0.76	1.91	0.99	0.81	0.91	0.83	0.49	0.23	0.23	0.23	0.15	0.26
Pb	31.40	27.85	32.03	35.67	36.44	27.29	49.70	50.19	42.66	24.31	28.43	29.56	29.65	23.93	26.29
Th	10.92	14.56	16.27	16.96	19.75	10.77	62.30	76.15	75.87	18.17	20.51	18.90	20.55	20.51	26.29
U	1.07	0.89	0.98	2.23	1.64	0.86	5.31	6.26	7.17	1.28	0.93	0.92	0.99	0.99	1.21
Y	12.57	7.28	7.71	11.49	12.65	9.44	18.48	22.84	21.86	13.53	12.47	11.54	11.36	9.39	13.25
La	16.65	23.95	22.87	18.91	29.08	10.76	60.17	74.34	73.79	43.88	74.54	72.10	63.64	68.37	77.27
Ce	34.99	45.43	43.57	37.42	56.49	24.20	118.85	147.26	146.66	108.73	150.62	149.76	138.35	150.57	169.34
Pr	3.84	4.76	4.63	3.95	6.00	2.62	15.29	18.85	18.86	10.20	17.83	17.15	15.23	16.17	18.53
Nd	13.06	17.48	17.03	15.20	22.25	9.63	45.87	57.20	56.81	34.17	51.08	49.55	43.79	46.16	53.35
Sm	2.33	2.96	2.97	3.02	3.97	1.92	8.10	10.02	10.01	4.96	7.35	7.16	6.38	6.56	7.93
Eu	0.60	0.53	0.55	0.59	0.60	0.39	1.00	1.12	1.08	1.05	1.08	1.07	1.06	1.01	1.02
Gd	2.18	2.29	2.35	2.84	3.19	1.83	5.98	7.25	7.31	4.42	4.69	4.49	4.00	4.10	5.22
Tb	0.30	0.33	0.35	0.46	0.49	0.32	0.84	1.03	1.02	0.53	0.68	0.63	0.58	0.60	0.77
Dy	1.69	1.67	1.76	2.41	2.48	1.80	3.97	4.87	4.78	2.84	3.20	3.02	2.83	2.85	3.62
Ho	0.30	0.28	0.31	0.42	0.44	0.35	0.71	0.86	0.82	0.51	0.54	0.50	0.48	0.47	0.58
Er	0.75	0.68	0.76	0.97	1.09	0.85	1.70	2.07	1.97	1.39	1.21	1.11	1.15	1.08	1.24
Tm	0.11	0.10	0.12	0.13	0.17	0.14	0.25	0.29	0.27	0.21	0.15	0.14	0.15	0.13	0.16
Yb	0.67	0.72	0.87	0.89	1.30	0.94	1.74	2.10	1.93	1.36	0.95	0.92	0.98	0.85	1.04
Lu	0.11	0.11	0.13	0.13	0.19	0.14	0.28	0.33	0.31	0.21	0.13	0.15	0.13	0.13	0.15
Hf	2.82	3.29	3.34	3.39	3.51	3.05	9.14	10.41	9.46	5.02	6.48	6.16	6.61	7.24	7.09

高,结晶于岩浆冷凝过程的早期,此时岩浆混合很可能尚不充分,因而锆石记录了不同岩浆混合端元的同位素成分,其中-9.4值可能来自富集的地壳端元,+1.9值则来自亏损的地幔端元;与此对应的是,全岩Nd同位素分析结果代表了岩浆充分混合

之后的同位素成分。本文倾向于第二种解释,原因如下:①前人研究表明,安多微陆块具有较古老的基底,其 $\epsilon_{\text{Hf}}(800 \text{ Ma})$ 可达-10左右(Liu Deliang et al., 2017),虽然地壳深熔作用过程中不同高场强元素富集矿物参与熔融比例不同可以一定程度上改

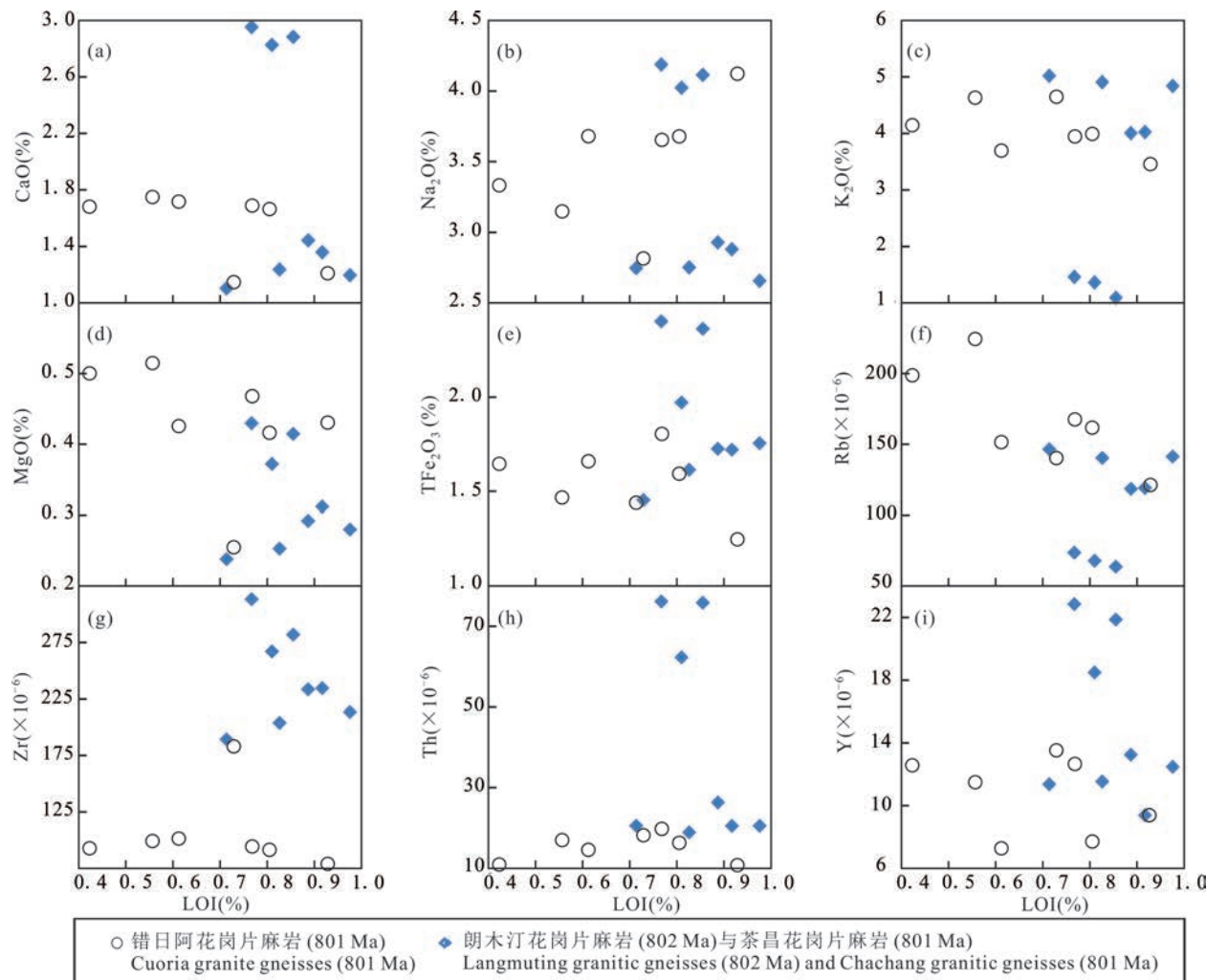


图 5 安多花岗片麻岩的典型活动元素(a、b、c、f),过渡元素(d、e)和不活动元素(g~i)与 LOI 的二元协变图解

Fig. 5 Plots of selected typical active elements (a, b, c, f), transitional elements (d, e) and inactive elements (g~i) vs. loss on ignition (LOI) of the granitic gneisses in the Amdo area

变 $\epsilon_{\text{Hf}}(t)$ 值的范围,但不可能出现由富集到亏损的转变,即不应该出现正 $\epsilon_{\text{Hf}}(t)$ 值的锆石;② 样品具有变化范围较大的 Ni 元素含量($1.36 \times 10^{-6} \sim 8.11 \times 10^{-6}$),其 $\text{Mg}^{\#}$ 值 [$100 \times \text{Mg}^{2+}/(\text{Mg}^{2+} + \text{Fe}^{2+})$] (26.8~45) 高于纯地壳熔体(图 8; Jiang Yaohui et al., 2013),也指示花岗质岩浆形成过程中存在幔源岩浆的参与。

哈克图解表明,花岗质岩浆形成后可能经历了结晶分异过程(图 7)。 Al_2O_3 随着 SiO_2 的增加而减少,表明其发生了长石的结晶分异作用。岩浆演化过程中 TiO_2 、 TiFe_2O_3 和 MgO 的减少表明岩浆演化晚期结晶过程中 Fe、Ti 矿物发生结晶分异。如前文所述, P_2O_5 含量降低应当与磷灰石分离有关。大多数样品的 Zr 随着 SiO_2 的增加而不断减少,这表明在其岩浆中是饱和的,这也受分离结晶的控制。

依据地球化学特征和矿物组成,花岗岩可以分为 I 型、S 型、M 型和 A 型(Chappell and White, 1974)。M 型花岗岩是洋壳的组成部分,一般具有低 Th 的特点,与本文研究的花岗片麻岩明显不同(图 4b)。P 含量是区分 I 型和 S 型花岗岩的重要标准,因为磷灰石在金属铝和轻度过铝质岩浆(I 型)中达到饱和,但磷灰石在强过铝质岩浆(S 型)中高度可溶(Wolf and London, 1994)。本文研究的花岗片麻岩 P_2O_5 含量较低(0.02%~0.06%),其 P_2O_5 含量与 SiO_2 含量呈负相关(图 8),且岩石薄片观察到少量角闪石矿物颗粒(图 2c),因而属于 I 型花岗岩。关于 I 型花岗岩的成因,目前主要有两种解释:① 地壳内变质火成岩的部分熔融作用(Chappell and White, 1974)和② 地幔岩浆对沉积物质的改造,即混染结晶分异过程(Kemp et al., 2007)。如

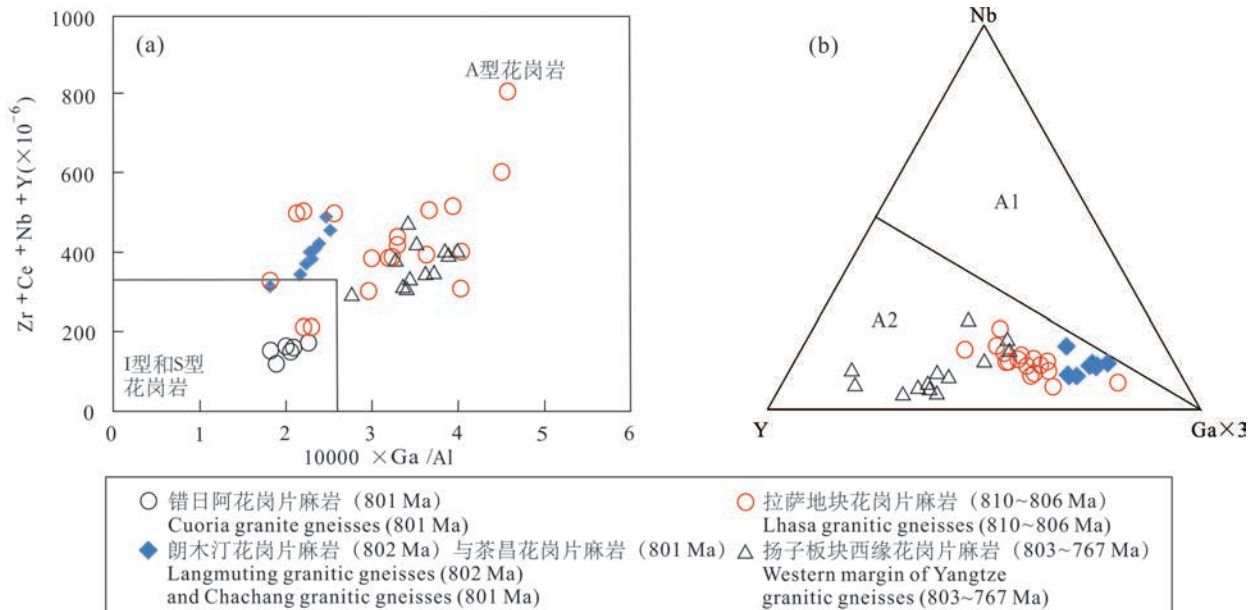


图 6 安多花岗片麻岩的 $Zr + Ce + Nb + Y$ 与 $10000 \times Ga/Al$ 判别图及 A 型花岗岩构造判别图

Fig. 6 $Zr + Ce + Nb + Y$ vs. $10000 \times Ga/Al$ discrimination diagram of the granitic gneisses and tectonic discrimination diagrams of the A-type granite in the Amdo area

数据资料引自 Li Xianhua et al., 2002b; Huang Xiaolong et al., 2008; Hu Peiyuan et al., 2018b 及其中参考文献

The data were quoted from Li Xianhua et al., 2002b; Huang Xiaolong et al., 2008; Hu Peiyuan et al., 2018b and their references

前文所述,同位素和地球化学资料指示这些花岗片麻岩样品成岩过程中有幔源岩浆的参与,因此本次研究倾向于第二种成因。此外,朗木汀花岗片麻岩(18T555-557)与茶昌花岗片麻岩(18T584-589)具有较高的高场强元素($Zr + Ce + Nb + Y$)含量($> 350 \times 10^{-6}$)(图 6a)和锆石饱和温度($> 800^\circ\text{C}$),因而兼具 A 型花岗岩的特征。关于这一地球化学特征,一种解释是可能与结晶分异过程相关,但是我们排除了这一可能,原因在于: $Zr + Nb + Ce + Y$ 含量和 Ga/Al 比值均与 SiO_2 呈负相关(图 7g,h),也就是结晶分异降低了 $Zr + Nb + Ce + Y$ 含量和 Ga/Al 比值,而不是升高。

4.3 构造环境

前人研究表明,I 型花岗岩几乎可能形成于各种构造环境,但是 A 型花岗岩只形成于与伸展相关的构造背景。Eby(1990, 1992)通过总结前人工作和分析大量典型构造背景下产出的 A 型花岗岩,将 A 型花岗岩划分为 A1 和 A2 两种类型,其中 A1 型代表了一种非造山环境(anorogenic),在大陆裂谷时期或板内岩浆作用(如热点、地幔柱的活动)侵入;A2 型形成的构造环境范围比较广泛,主要是后碰撞伸展环境(post-orogenic)。新近的研究成果表明 A2 型花岗岩也可以形成于岛弧环境,例如板片

俯冲引起的岩石圈伸展环境(周红升等,2008; 郭芳放等,2008; 蒋少涌等,2008; Huang He et al., 2012)。

如图 6b 所示,朗木汀与茶昌花岗片麻岩样品投图落入 A2 型的范围。由于 A2 型花岗岩形成的构造环境范围比较广泛,所以要确定其形成的构造环境必须与区域地质背景相结合。安多微陆块在构造位置上夹持在羌南-保山地块、拉萨地块和扬子板块之间,其新元古代演化历史与这些相邻陆块密切相关。前人在与安多微陆块相邻的拉萨地块(810~806 Ma)和扬子西缘地区(803~767 Ma)均发现了同时代的 A2 型花岗岩(Li Xianhua et al., 2002b; Huang Xiaolong et al., 2008; Hu Peiyuan et al., 2018b)。羌南-保山地块上虽然暂时没有发现同时代的 A 型花岗岩,但是在新元古代晚期火山岩中发现了大量的约 800 Ma 继承锆石(Wang Ming et al., 2015)。这些资料指示在我国西南地区存在规模巨大的一期约 800 Ma 岩浆事件。这一岩浆事件不仅包括本次研究识别出的安多花岗片麻岩,还包括大量与弧后拉张相关的岩浆记录,例如: Hu Peiyuan et al. (2018b) 在拉萨地块上识别出了约 822 Ma 的变质基性岩,这些岩石兼具 MORB(平缓的稀土元素和微量元素配分曲线)和岛弧岩浆岩(偏

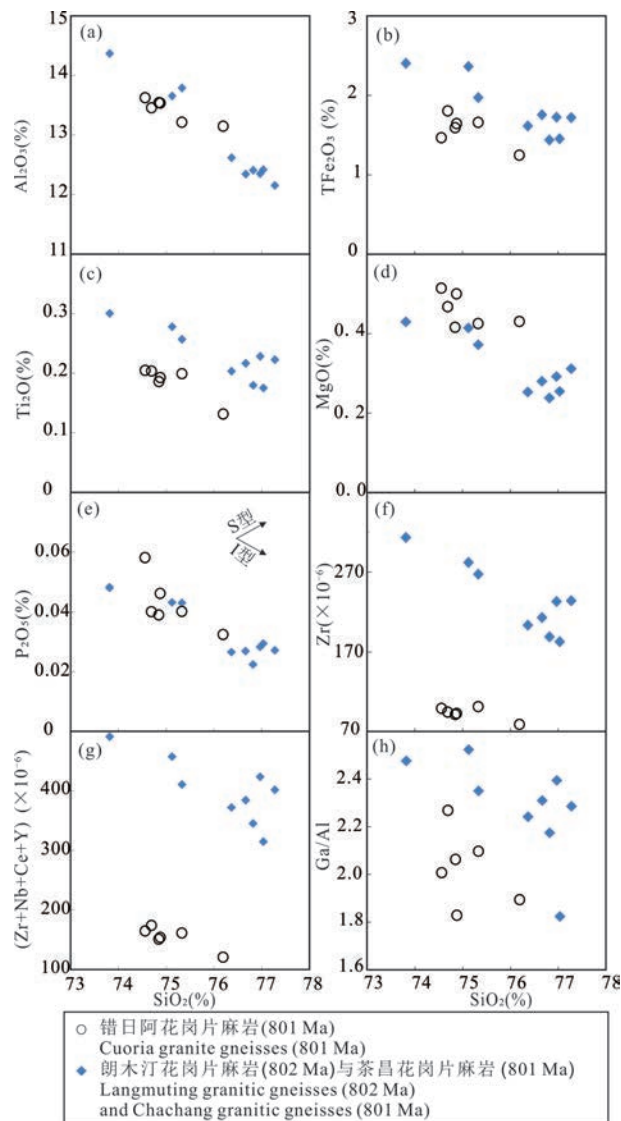
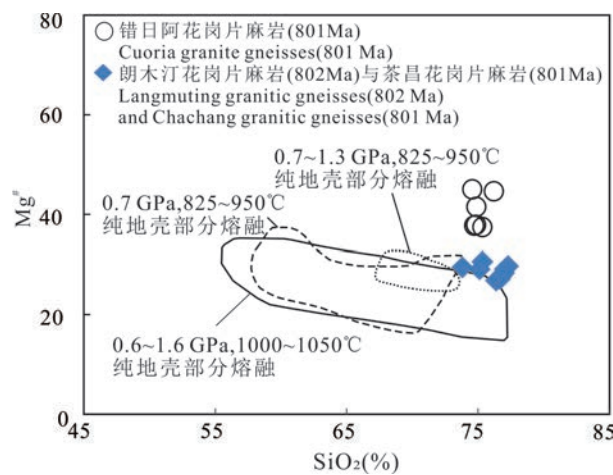


图 7 安多地区花岗片麻岩的哈克图解

Fig. 7 Harker diagrams of the granitic gneisses in the Amdo area

高的 Th/Yb 比值)的地球化学特征,符合弧后盆地岩浆岩的特征(图 9)。类似的基性岩浆岩也出露于扬子西缘的盐边地区(图 9; Sun Weihua et al., 2007; Zhou Meifu et al., 2006)。此外, Zhao Junhong et al. (2011)对扬子地块内部南华盆地沉积岩开展了精确的定年研究,结果显示南华盆地打开于约 830~725 Ma,与扬子西缘的岛弧岩浆事件具有时间和空间上的一致性,很可能是一个弧后盆地,从而为中国西南地区存在约 800 Ma 弧后拉张事件提供了直接证据。与此对应的是,在中国西南地区并未发现近同时代的陆-陆碰撞事件。前人报道拉萨地块陆-陆碰撞成因的高压麻粒岩的峰期变质时代约为 650 Ma(Zhang Zeming et al., 2012b)。

图 8 安多花岗片麻岩的 Mg[#] 与 SiO₂ 判别图

(据 Jiang Yaohui et al., 2013)

Fig. 8 Mg[#] vs. SiO₂ diagram of the granitic gneisses in the Amdo area (modified after Jiang Yaohui et al., 2013)

受控于江南造山带的碰撞闭合,在扬子陆块上虽然发育约 800 Ma 的陆-陆碰撞事件,但是其岩浆记录主要位于扬子地块东部,远离安多微陆块(Zhang Chuanlin et al., 2013)。综上,本文倾向于将安多花岗片麻岩解释为弧后盆地环境。

4.4 安多微陆块古地理位置

拉伸纪岩浆岩广泛分布于罗迪尼亞超大陆的几个大陆地块中,包括澳洲(Zhao Jianxin et al., 1994)、劳伦(Heaman et al., 1992; Milton et al., 2017; Cox et al., 2018)、华南(Li Xianhua et al., 2002a, 2002b; Huang Xiaolong et al., 2008)、印度(例如,Torsvik et al., 2001; Singh et al., 2006; Wang Yuejun et al., 2018)和塔里木(Zhang Zhaochong et al., 2012; Wu Guanghui et al., 2018; Liao Fanxi et al., 2018)陆块。这些岩石与安多微陆块上同时代岩浆岩的对比为我们探索其前寒武纪起源提供了线索。

罗迪尼亞超大陆内部的大多数拉伸纪岩浆岩都被认为形成于导致超大陆产生裂谷和破裂的超级地幔柱(Heaman et al., 1992; Zhao Jianxin et al., 1994; Li Zhengxiang et al., 1999; Li Xianhua et al., 2002a, 2002b, 2008; Frimmel et al., 2001; Shellnutt et al., 2004; Maruyama et al., 2007)。典型的岩浆岩以甘巴雷尔(Gunbarrel)岩浆事件(约 780 Ma; Sandeman et al., 2014; Milton et al., 2017)、富兰克林(Franklin)大火成岩省(约 720 Ma; Heaman et al., 1992; Cox et al., 2018)和盖尔德

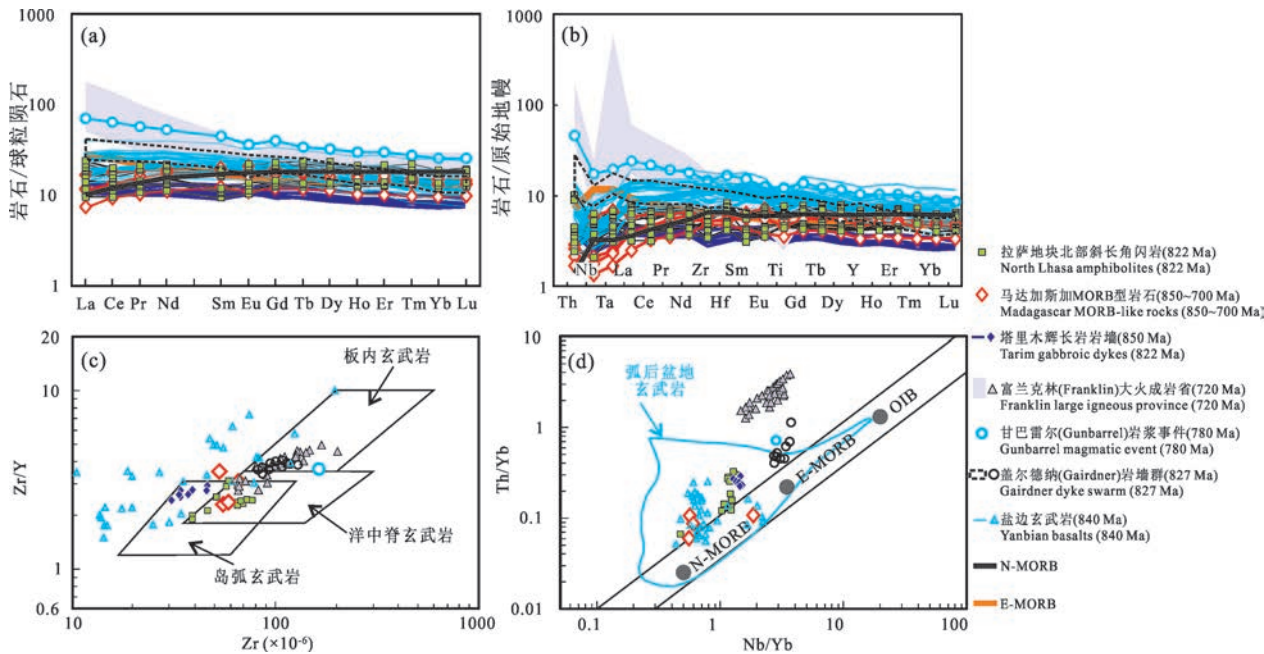


图 9 安多周边地区基性岩与罗迪尼亞超大陆内部典型岩浆岩的球粒陨石标准化稀土元素配分图(a)和原始地幔标准化微量元素蛛网图(b)(标准化值据 Sun and McDonough, 1989)及构造环境判别图(c)(d)

Fig. 9 Chondrite-normalized REE (a), primitive mantle-normalized trace element (b) (normalization values are after Sun and McDonough, 1989) and tectonic discrimination diagrams of the mafic rocks around the Amdo area and the typical magmatic rocks inside the Rodinia

数据资料引自 Zhao Jianxin et al., 1994; Zhou Meifu et al., 2006; Jöns and Schenk, 2008; Milton et al., 2017; Cox et al., 2018; Liao Fanxi et al., 2018; Hu Peiyuan et al., 2018b

The data were quoted from Zhao Jianxin et al., 1994; Zhou Meifu et al., 2006; Jöns and Schenk, 2008; Milton et al., 2017; Cox et al., 2018; Liao Fanxi et al., 2018; Hu Peiyuan et al., 2018b

纳(Gairdner)岩墙群(约 827 Ma; Zhao Jianxin et al., 1994)为代表(图 10)。这些岩石主要是玄武质岩石,其特征是富集岩浆源区和明显受地壳混染(Zhao Jianxin et al., 1994; Milton et al., 2017; Cox et al., 2018),普遍具有明显右倾的稀土元素和微量元素配分曲线,在构造环境判别图中落入板内玄武岩区域(图 9a~c)。本研究中的花岗片麻岩产生于岛弧环境,为与俯冲相关的岩浆作用,与罗迪尼亞超大陆内部的古地理位置不符。

罗迪尼亞超大陆的分裂与其周围的洋壳俯冲有关(Li Zhengxiang et al., 1999; Li Xianhua et al., 2008; Cawood et al., 2017)。由于这些俯冲作用,在罗迪尼亞超大陆的西北缘发生了活跃的安第斯型造山运动(Torsvik et al., 1996; Meert and Torsvik, 2003; Gregory et al., 2009; Bybee et al., 2010)。在印度西部(约 769~762 Ma; Torsvik et al., 2001; Singh et al., 2006; Wang Yuejun et al., 2018)、塞舌尔(约 809~748 Ma; Torsvik et al., 2001; Singh et al., 2006; Wang Yuejun et al., 2018)、马达加斯加(约 850~700 Ma; Jöns and Schenk, 2008; Archibald et al., 2016)和中国塔里木(约 850 Ma; Wu Guanghui et al., 2018)均发现了拉伸纪安第斯型岩浆岩。尽管中国华南地块中广泛存在的新元古代双峰岩浆作用被认为与大陆裂谷环境有关(Li Xianhua et al., 2008),但在该地块中也发现了与拉伸纪安第斯型造山运动相关的岩浆作用(Zhou Meifu et al., 2002, 2006; Du Lilin et al., 2014)。值得注意的是,由于超大陆边缘俯冲大洋板片的回撤,几个弧后盆地在约 800 Ma 时开启。典型的弧后盆地玄武岩出现在马达加斯加(约 850~700 Ma; Jöns and Schenk, 2008)和中国塔里木地区(约 850 Ma; Liao Fanxi et al., 2018),它们普遍具有平缓的稀土元素和微量元素配分曲线,在构造环境判别图中落入 MORB 或者岛弧玄武岩区域,与中国西南地区约 800 Ma 弧后盆地基性岩类似(图 9)。在弧后伸展构造背景下,马达加斯加(约 790~780 Ma; Nédélec et al., 2016)、中国华南(约 803~767 Ma; Li Xianhua et al., 2002b; Huang

al., 2018)、马达加斯加(约 850~700 Ma; Jöns and Schenk, 2008; Archibald et al., 2016)和中国塔里木(约 850 Ma; Wu Guanghui et al., 2018)均发现了拉伸纪安第斯型岩浆岩。尽管中国华南地块中广泛存在的新元古代双峰岩浆作用被认为与大陆裂谷环境有关(Li Xianhua et al., 2008),但在该地块中也发现了与拉伸纪安第斯型造山运动相关的岩浆作用(Zhou Meifu et al., 2002, 2006; Du Lilin et al., 2014)。值得注意的是,由于超大陆边缘俯冲大洋板片的回撤,几个弧后盆地在约 800 Ma 时开启。典型的弧后盆地玄武岩出现在马达加斯加(约 850~700 Ma; Jöns and Schenk, 2008)和中国塔里木地区(约 850 Ma; Liao Fanxi et al., 2018),它们普遍具有平缓的稀土元素和微量元素配分曲线,在构造环境判别图中落入 MORB 或者岛弧玄武岩区域,与中国西南地区约 800 Ma 弧后盆地基性岩类似(图 9)。在弧后伸展构造背景下,马达加斯加(约 790~780 Ma; Nédélec et al., 2016)、中国华南(约 803~767 Ma; Li Xianhua et al., 2002b; Huang

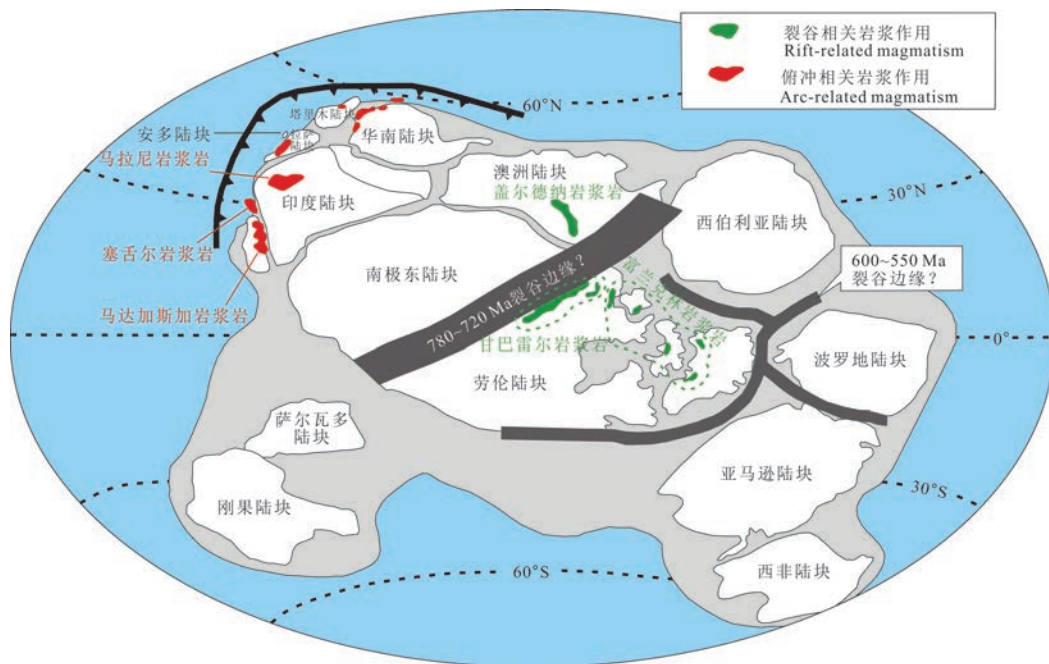


图 10 罗迪尼亚超大陆重建图(据 Meert and Torsvik, 2003)

Fig. 10 Reconstruction of Rodinia supercontinent showing the oceanic subduction system along the northwestern margin of Rodinia (modified after Meert and Torsvik, 2003)

Xiaolong et al., 2008) 和印度西部马拉尼 (Malani; 约 790~762 Ma; Wang Yuejun et al., 2018) 形成了许多 A2 型花岗质岩石。这些花岗质岩石在地球化学上与本研究的同时代花岗片麻岩具有可比性, 因此本文推测安多微陆块可能位于罗迪尼亚超大陆的西北边缘, 靠近马达加斯加、塞舌尔和印度西部 (图 10)。

5 结论

综合上述分析讨论, 初步得出以下结论:

(1) 安多花岗片麻岩锆石 LA-ICP-MS U-Pb 定年结果为 802~801 Ma, 时代为拉伸纪。

(2) 地球化学特征显示, 安多花岗片麻岩原岩属于 I 型花岗岩并兼具 A 型花岗岩的特征。不均匀的锆石 Hf 和相对均匀的全岩 Nd 同位素成分 ($\epsilon_{\text{Hf}}(t) = -9.4 \sim +1.9$; $\epsilon_{\text{Nd}}(t) = -4.8 \sim -3.4$) 以及古老的地壳模式年龄 (2289~1575 Ma), 指示岩石可能形成于幔源岩浆对元古宙地壳的改造, 随后经历了广泛的结晶分异过程。

(3) 中国安多花岗片麻岩可能形成于弧后拉张环境, 与马达加斯加、塞舌尔和印度西部的拉伸纪岩浆记录可对比, 指示安多微陆块此时可能位于罗迪尼亚超大陆的西北边缘。

致谢:感谢审稿人对本文提出的中肯的、建设性

的修改意见;感谢朱志才、王伟和吴昊在野外考察过程中的帮助;全岩地球化学分析、锆石 U-Pb 定年和全岩 Sr-Nd 同位素分析得到了北京科荟测试技术有限公司孔德为工程师的帮助;锆石 Hf 同位素分析得到了中国科学院地质与地球物理研究所李娇实验师的帮助。在此一并致以衷心的感谢。

References

- Archibald D B, Collins A S, Foden J D, Payne J L, Holden P, Razakamanana T, Waele B D, Thomas R J, Pitfield P E J. 2016. Genesis of the Tonian ImoronaItsindro magmatic suite in central Madagascar: Insights from U-Pb, oxygen and hafnium isotopes in zircon. *Precambrian Research*, 281: 312~337.
- Bybee G M, Ashwal L D, Wilson A H. 2010. New evidence for a volcanic arc on the western margin of a rifting Rodinia from the ultramafic intrusions in the Andriamena region, north-central Madagascar. *Earth and Planetary Science Letters*, 293(1-2): 42~53.
- Cawood P A, Pisarevsky S A. 2017. Laurentia-Baltica-Amazonia relations during Rodinia assembly. *Precambrian Research*, 292: 386~397.
- Chappell B W, White A J R. 1974. Two contrasting granite types. *Pacific Geology*, 8: 173~174.
- Collins A S, Pisarevsky S A. 2005. Amalgamating eastern Gondwana: The evolution of the Circum-Indian Orogens. *Earth-Science Reviews*, 71(3-4): 229~270.
- Cox G M, Halversong G P, Denysynd S, Foden J, Macdonald F A. 2018. Cryogenian magmatism along the north-western margin of Laurentia: Plume or rift? *Precambrian Research*, 319: 144~157.
- Dalziel I W D. 1991. Pacific margins of Laurentia and East Antarctic-Australia as a conjugate rift pair: Evidence and implications for an Eocambrian supercontinent. *Geology*, 19: 598~601.

- Ding Huixia, Zhang Zeming, Dong Xin, Yan Rong, Lin Yanhao, Jiang Hongying. 2015. Cambrian ultrapotassic rhyolites from the Lhasa terrane, south Tibet: Evidence for Andean-type magmatism along the northern active margin of Gondwana. *Gondwana Research*, 27(4): 1616~1629.
- Dong Xin, Zhang Zeming, Santosh M, Wang Wei, Yu Fei, Liu Feng. 2011. Late Neoproterozoic thermal events in the northern Lhasa terrane, south Tibet: Zircon chronology and tectonic implications. *Journal of Geodynamics*, 52 (5): 389~405.
- Du Lilin, Guo Jinghui, Nutman A P, Wyman D, Geng Yuansheng, Yang Chonghui, Liu Fulai, Ren Liudong, Zhou Xiwen. 2014. Implications for Rodinia reconstructions for the initiation of Neoproterozoic subduction at ~860 Ma on the western margin of the Yangtze Block: Evidence from the Guandaoshan Pluton. *Lithos*, 196: 67~82.
- Eby G N. 1990. The A-type granitoids: A review of their occurrence and chemical characteristics and speculations on their petrogenesis. *Lithos*, 26: 115~134.
- Eby G N. 1992. Chemical subdivision of the A-type granitoids: petrogenetic and tectonic implications. *Geology*, 20: 641~644.
- Frimmel H E, Zartman R, Späth E. 2001. The Richtersveld igneous complex, South Africa: U-Pb zircon and geochemical evidence for the beginning of Neoproterozoic continental breakup. *The Journal of Geology*, 109(4): 493~508.
- Goodge J W, Vervoort J D, Fanning C M, Brecke D M, Farmer G L, Williams I S, Myrow P M, DePaolo D J. 2008. A positive test of East Antarctica-Laurentia juxtaposition within the Rodinia supercontinent. *Science*, 321(5886): 235~240.
- Gregory L C, Meert J G, Bingen B, Pnadir M K, Torsvik T H. 2009. Paleomagnetism and geochronology of the Malani Igneous Suite, Northwest India: Implications for the configuration of Rodinia and the assemblage of Gondwana. *Precambrian Research*, 170(1-2): 13~26.
- Guo Fangfang, Jiang Changyi, Su Chunqian, Xia Mingzhe, Xia Zhaoe, Wei Wei. 2008. Tectonic settings of A-type granites of Shaerdan area, southeastern margin of Junggar block, Xinjiang, western China. *Acta Petrologica Sinica*, 24 (12): 2778~2788 (in Chinese with English abstract).
- Guynn J, Kapp P, Gehrels G E, Ding Lin. 2012. U-Pb geochronology of basement rocks in central Tibet and paleogeographic implications. *Journal of Asian Earth Sciences*, 43(1): 23~50.
- Hart S R, Staudigel H. 1982. The control of alkalis and uranium in seawater by ocean crust alteration. *Earth and Planetary Science Letters*, 58(2): 202~212.
- Heaman L M, LeCheminant A N, Rainbird R H. 1992. Nature and timing of Franklin igneous events, Canada: Implications for a Late Proterozoic mantle plume and the break-up of Laurentia. *Earth and Planetary Science Letters*, 109(1-2): 117~131.
- Hoffman F P. 1991. Did breakout of Laurentia turn Gondwana inside-out? *Science*, 252: 1409~1411.
- Hou Kejun, Li Yanhe, Tian Yourong. 2009. *In situ* U-Pb zircon dating using laser ablation-multi ion counting-ICP-MS. *Mineral Deposits*, 28 (4): 481~492 (in Chinese with English abstract).
- Hu Daogong, Wu Zhenhan, Jiang Wan, Shi Yuruo, Ye Peisheng, Liu Qisheng. 2005. SHRIMP zircons from Nianqing Tanggula Group, Tibet: Studies on U-Pb age and Nd isotope. *Science in China, Earth Science*, 35(1): 29~37 (in Chinese with English abstract).
- Hu Peiyuan, Zhai Qingguo, Wang Jun, Tang Yue, Wang Haitao, Zhu Zhicai, Wu Hao. 2018a. Middle Neoproterozoic (ca. 760 Ma) arc and back-arc system in the North Lhasa terrane, Tibet, inferred from coeval N-MORB and arc-type gabbros. *Precambrian Research*, 316: 275~290.
- Hu Peiyuan, Zhai Qingguo, Wang Jun, Tang Yue, Wang Haitao, Hou Kejun. 2018b. Precambrian origin of the North Lhasa terrane, Tibetan Plateau: Constraint from early Cryogenian back-arc magmatism. *Precambrian Research*, 313: 51~67.
- Hu Peiyuan, Zhai Qingguo, Zhao Guochun, Wang Jun, Tang Yue, Wang Haitao, Zhu Zhicai, Wang Wei, Wu Hao. 2018c. Early Neoproterozoic (ca. 900 Ma) rift sedimentation and mafic magmatism in the North Lhasa terrane, Tibet: Paleogeographic and tectonic implications. *Lithos*, 320: 403~415.
- Hu Peiyuan, Zhai Qingguo, Ren Guangming, Wang Jun, Tang Yue. 2018d. Late Ordovician high-Mg adakitic andesite in the western South China block: Evidence of oceanic subduction. *International Geology Review*, 60(9): 1140~1154.
- Hu Peiyuan, Zhai Qingguo, Zhao Guochun, Wang Jun, Tang Yue, Wang Haitao, Zhu Zhicai, Wu Hao, Wang Wei, Huang Zhiqiang. 2019a. Late Cryogenian magmatic activity in the North Lhasa terrane, Tibet: Implication of slab break-off process. *Gondwana Research*, 71: 129~149.
- Hu Peiyuan, Zhai Qingguo, Zhao Guochun, Wang Jun, Tang Yue, Zhu Zhicai, Wu Hao. 2019b. The North Lhasa terrane in Tibet was attached with the Gondwana before it was drafted away in Jurassic: evidence from detrital zircon studies. *Journal of Asian Earth Sciences*, 185: 104055.
- Hu Peiyuan, Zhai Qingguo, Zhao Guochun, Wang Jun, Tang Yue, Zhu Zhicai, Wang Wei, Wu Hao. 2021. Cambrian and Cryogenian tectonothermal events in the Amdo microcontinent, Central Tibet: Implications for paleogeographic reconstruction and tectonic evolution of northern Gondwana. *Palaeogeography, Palaeoclimatology, Palaeoecology*, 569: 110332.
- Hu Peiyuan, Zhai Qingguo, Cawood P A, Zhao Guochun, Wang Jun, Tang Yue, Zhu Zhicai, Wang Wei, Wu Hao. 2022. Middle Neoproterozoic (ca. 700 Ma) tectonothermal events in the Lhasa terrane, Tibet: Implications for paleogeography. *Gondwana Research*, 104: 252~264.
- Huang He, Zhang Zhaochong, Kusky T, Santosh M, Zhang Shu, Zhang Dongyang, Liu Junlai, Zhao Zhidan. 2012. Continental vertical growth in the transitional zone between South Tianshan and Tarim, western Xinjiang, NW China: Insight from the Permian Halajun A1-type granitic magmatism. *Lithos*, 155: 49~66.
- Huang Xiaolong, Xu Yigang, Li Xianhua, Li Wuxian, Lan Jiangbo, Zhang Huihuang, Liu Yongsheng, Wang Yanbin, Li Hongyan, Luo Zhengyu, Yang Qijun. 2008. Petrogenesis and tectonic implications of Neoproterozoic, highly fractionated A-type granites from Mianning, South China. *Precambrian Research*, 165: 190~204.
- Jackson S E, Pearson N J, Griffin W L, Belousova E A. 2004. The application of laser ablation-inductively coupled plasma-mass spectrometry to *in situ* U-Pb zircon geochronology. *Chemical Geology*, 211(1-2): 47~69.
- Jiang Shaoyong, Zhao Kuidong, Jiang Yaohui, Dai Baozhang. 2008. Characteristics and genesis of Mesozoic A-type granites and associated mineral deposits in the southern Hunan and northern Guangxi Provinces along the Shi-Hang belt, South China. *Geological Journal of China Universities*, 14 (4): 496~509 (in Chinese with English abstract).
- Jiang Yaohui, Jia Ruya, Liu Zheng, Liao Shiyong, Zhao Peng, Zhou Qing. 2013. Origin of Middle Triassic high K calc-alkaline granitoids and their potassic microgranular enclaves from the western Kunlun orogeny, Northwest China: A record of the closure of Paleo-Tethys. *Lithos*, 156: 13~30.
- Jóns N, Schenk V. 2008. Relics of the Mozambique Ocean in the central East African Orogen: Evidence from the Vohibory Block of southern Madagascar. *Journal of Metamorphic Geology*, 26 (1): 17~28.
- Kemp A I S, Hawkesworth C J, Foster G L, Paterson B A, Woodhead J D, Hergt J M, Gray C M, Whitehouse M J. 2007. Magmatic and crustal differentiation history of granitic rocks from Hf-O isotopes in zircon. *Science*, 315(5814): 980~983.
- Li Xianhua, Li Zhengxiang, Ge Wenchun, Zhou Hanwen, Li Wuxian, Liu Ying, Wingate M T D. 2002a. Neoproterozoic granitoids in South China: Crustal melting above a mantle

- plume at ca. 825 Ma? *Precambrian Research*, 122(1-4): 45~83.
- Li Xianhua, Li Zhengxiang, Zhou Hanwen, Liu Ying, Kinny P D. 2002b. U-Pb zircon geochronology, geochemistry and Nd isotopic study of Neoproterozoic bimodal volcanic rocks in the Kangdian rift of South China: implications for the initial rifting of Rodinia. *Precambrian Research*, 113(1-2): 135~154.
- Li Xianhua, Li Wuxian, Li Zhengxiang, Liu Ying. 2008. 850~790 Ma bimodal volcanic and intrusive rocks in northern Zhejiang, South China: A major episode of continental rift magmatism during the breakup of Rodinia. *Lithos*, 102(1-2): 341~357.
- Li Zhengxiang, Li Xianhua, Kinny P D, Wang J. 1999. The breakup of Rodinia: Did it start with a mantle plume beneath South China? *Earth and Planetary Science Letters*, 173(3): 171~181.
- Li Zhengxiang, Bogdanova S V, Collins A, Davidson A, De Waele B, Ernst R E, Fitzsimons I, Fuck R, Gladkochub D, Jacobs J, Karlstrom K, Lu S, Milesi J P, Myers J, Natapov L, Pandit M, Pease V, Pisarevsky S A, Thrane K, Vernikovsky. 2008. Assembly, configuration, and break-up history of Rodinia: a synthesis. *Precambrian Research*, 160(1-2): 179~210.
- Liao Fanxi, Wang Qinyan, Chen Nengsong, Santosh M, Xu Yixian, Mustafa H A. 2018. Geochemistry and geochronology of the ~ 0.82 Ga high-Mg gabbroic dykes from the Quanji Massif, southeast Tarim Block, NW China: Implications for the Rodinia supercontinent assembly. *Journal of Asian Earth Sciences*, 157: 3~21.
- Liu Deliang, Shi Rendeng, Ding Lin, Huang Qishuai, Zhang Xiaoran, Yue Yahui, Zhang Liyun. 2017. Zircon U-Pb age and Hf isotopic compositions of Mesozoic granitoids in southern Qiangtang, Tibet: Implications for the subduction of the Bangong-Nujiang Tethyan Ocean. *Gondwana Research*, 41: 157~172.
- Li Pu. 1955. A preliminary understanding of geology in eastern Tibet. *Chinese Science Bulletin*, (7): 62~71 (in Chinese with English abstract).
- Liu Yongsheng, Gao Shan, Hu Zhaochu, Gao Changgui, Zong Keping, Wang Dongbing. 2010. Continental and oceanic crust recycling-induced melt-peridotite interactions in the Trans-North China Orogen: U-Pb dating, Hf isotopes and trace elements in zircons from mantle xenoliths. *Journal of Petrology*, 51(1-2): 537~571.
- Ludwig K R. 2003. Isoplot 3.00: A Geochronological Toolkit for Microsoft Excel. Berkeley: Berkeley Geochronology Center Special Publication, 4: 70.
- Maruyama S, Santosh M, Zhao D. 2007. Superplume, supercontinent, and post-perovskite: Mantle dynamics and antiplate tectonics on the core-mantle boundary. *Gondwana Research*, 11(1-2): 7~37.
- Meert J G, Torsvik T H. 2003. The making and unmaking of a supercontinent: Rodinia revisited. *Tectonophysics*, 375(1-4): 261~288.
- Milton J E, Hickey K A, Gleeson S A, Friedman R M. 2017. New U-Pb constraints on the age of the Little Dal basalts and Gunbarrel-related volcanism in Rodinia. *Precambrian Research*, 296: 168~180.
- Mo Xuanxue, Dong Guochen, Zhao Zhidan, Zhou Su, Wang Liangliang, Qiu Ruzhao, Zhang Fengqin. 2005. Spatial and temporal distribution and characteristics of granitoids in the Gangdese Tibet and implication for crustal growth and evolution. *Geological Journal of China Universities*, 11 (3): 281~290 (in Chinese with English abstract).
- Moores E M. 1991. Southwest U. S.—East Antarctic (SWEAT) connection: A hypothesis. *Geology*, 19: 425~428.
- Nédélec A, Paquette J L, Antonio P, Paris G, Bouchez J L. 2016. A-type stratoid granites of Madagascar revisited: Age, source and links with the breakup of Rodinia. *Precambrian Research*, 280: 231~248.
- Pan Guitang, Mo Xuanxue, Hou Zengqian, Zhu Dicheng, Wang Liquan, Li Guangming, Zhao Zhidan, Geng Quanru, Liao Zhongli. 2006. Spatial-temporal framework of the Gangdese Orogenic belt and its evolution. *Acta Petrologica Sinica*, 22 (3): 521~533 (in Chinese with English abstract).
- Sandeman H A, Ootes L, Cousens B, Kilian T. 2014. Petrogenesis of Gunbarrel magmatic rocks: Homogeneous continental tholeiites associated with extension and rifting of Neoproterozoic Laurentia. *Precambrian Research*, 252: 166~179.
- Shellnutt J G, Dostal J, Keppie J D. 2004. Petrogenesis of the 723 Ma Coronation sills, Amundsen basin, Arctic Canada: Implications for the breakup of Rodinia. *Precambrian Research*, 129(3-4): 309~324.
- Singh A K, Singh R K B, Vallinayagam G. 2006. Anorogenic acid volcanic rocks in the Kundal area of the Malani igneous suite, northwestern India: Geochemical and petrogenetic studies. *Journal of Asian Earth Sciences*, 27(4): 544~557.
- Sun S S, McDonough W F. 1989. Chemical and isotopic systematics of oceanic basalts: Implications for mantle composition and processes. *Geological Society, London, Special Publications*, 42 (1): 313~345.
- Sun Weihua, Zhou Meifu, Zhao Junhong. 2007. Geochemistry and tectonic significance of basaltic lavas in the Neoproterozoic Yanbian Group, southern Sichuan Province, southwest China. *International Geology Review*, 49(6): 554~571.
- Torsvik T H. 2003. The Rodinia jigsaw puzzle. *Science*, 300 (5624): 1379~1381.
- Torsvik T H, Smethurst M A, Meert J G, Van der Voo R, McKerrow W S, Brasier M D, Sturt B A, Walderhaug H J. 1996. Continental break-up and collision in the Neoproterozoic and Palaeozoic—A tale of Baltica and Laurentia. *Earth-Science Reviews*, 40(3-4): 229~258.
- Torsvik T H, Carter L M, Ashwal L D, Bhushan S K, Pandit M K, Jamtveit B. 2001. Rodinia refined or obscured: palaeomagnetism of the Malani igneous suite (NW India). *Precambrian Research*, 108(3-4): 319~333.
- Verma S P. 1981. Seawater alteration effects on ^{87}Sr , ^{86}Sr , K, Rb, Cs, Ba and Sr in oceanic igneous rocks. *Chemical Geology*, 34 (1-2): 81~89.
- Wang Ming, Li Cai, Xie Chaoming, Wu Yanwang, Su Li, Hu Peiyuan. 2012. LA-ICP-MS U-Pb dating of zircon from granitic gneiss of the Nierong microcontinent: The discovery of the Neoproterozoic basement rock and its significance. *Acta Petrologica Sinica*, 28 (12): 4101~4108 (in Chinese with English abstract).
- Wang Ming, Li Cai, Fan Jianjun. 2015. Geochronology and geochemistry of the Dabure basalts, central Qiangtang, Tibet: Evidence for ~ 550 Ma rifting of Gondwana. *International Geology Review*, 57(14): 1791~1805.
- Wang Yuejun, Qian Xin, Cawood P A, Liu Huichuan, Feng Qinglai, Zhao Guochun, Zhang Yanhua, He Huiying, Zhang Peizhen. 2018. Closure of the East Paleotethyan Ocean and amalgamation of the eastern cimmerian and Southeast Asia continental fragments. *Earth- Science Review*, 186: 195~230.
- Wolf M B, London D. 1994. Apatite dissolution into peraluminous haplogranitic melts: An experimental study of solubilities and mechanisms. *Geochimica et Cosmochimica Acta*, 58(19): 4127~4145.
- Wu Fuyuan, Yang Yueheng, Xie Liewen, Yang Jinhui, Xu Ping. 2006. Hf isotopic compositions of the standard zircons and baddeleyites used in U-Pb geochronology. *Chemical Geology*, 234(1-2): 105~126.
- Wu Fuyuan, Li Xianhua, Zheng Yongfei, Gao Shan. 2007. Lu-Hf isotopic systematics and their applications in petrology. *Acta Petrologica Sinica*, 23 (2): 185~220 (in Chinese with English abstract).
- Wu Guanghui, Xiao Yang, Bonin B, Ma Debo, Li Xin, Zhu Guangyou. 2018. Ca. 850 Ma magmatic events in the Tarim Craton: Age, geochemistry and implications for assembly of Rodinia supercontinent. *Precambrian Research*, 305: 489

- ~503.
- Wu Yuanbao, Zheng Yongfei. 2004. Zircon genetic mineralogy and its restriction on U-Pb age interpretation. Chinese Science Bulletin, 49 (16): 1589~1604 (in Chinese with English abstract).
- Xie Chaoming, Li Cai, Wang Ming, Wu Yanwang, Hu Zhaochu. Tectonic affinity of the Nyainrong microcontinent: Constraints from zircon U-Pb age and Hf isotopes compositions. Geological Bulletin of China, 33 (11): 1778~1792 (in Chinese with English abstract).
- Yang Tiannan, Zhang Hongrui, Liu Y X, Wang Z L, Song Y C, Yang Z S, Tian S H, Xie H Q, Hou K J. 2011. Permo-Triassic arc magmatism in central Tibet: Evidence from zircon U-Pb geochronology, Hf isotopes, rare earth elements, and bulk geochemistry. Chemical Geology, 284(3-4): 270~282.
- Yang Tiannan, Ding Yijuan, Zhang Hongrui, Fan J W, Liang Mingjuan, Wang X H. 2014. Two-phase subduction and subsequent collision defines the Paleotethyan tectonics of the southeastern Tibetan Plateau: evidence from zircon U-Pb dating, geochemistry, and structural geology of the Sanjiang orogenic belt, southwest China. GSA Bulletin, 126 (11-12): 1654~1682.
- Yin An, Harrison T M. 2000. Geologic evolution of the Himalayan-Tibetan orogen. Annual Review of Earth and Planetary Sciences, 28(1): 211~280.
- Zhai Qingguo, Jahn B M, Wang Jun, Su Li, Mo Xuanxue, Wang Kuolung, Tang Suohan, Lee Haoyang. 2013. The Carboniferous ophiolite in the middle of the Qiangtang terrane, Northern Tibet: SHRIMP U-Pb dating, geochemical and Sr-Nd-Hf isotopic characteristics. Lithos, 168: 186~199.
- Zhai Qingguo, Jahn B M, Wang Jun, Hu Peiyuan, Chung Sunlin, Lee Haoyang, Tang Suohan, Tang Yue. 2016. Oldest paleo-Tethyan ophiolitic mélange in the Tibetan Plateau. Bulletin, 128(3-4): 355~373.
- Zhang Chuanlin, Santosh M, Zou Haibo, Li Huaikun, Huang Wencheng. 2013. The Fuchuan ophiolite in Jiangnan orogen: Geochemistry, zircon U-Pb geochronology, Hf isotope and implications for the Neoproterozoic assembly of South China. Lithos, 179: 263~274.
- Zhang Zhaochong, Kang Jianli, Kusky T, Santosh M, Huang He, Zhang Dongyang, Zhu Jiang. 2012. Geochronology, geochemistry and petrogenesis of Neoproterozoic basalts from Sugetbrak, northwest Tarim block, China: Implications for the onset of Rodinia supercontinent breakup. Precambrian Research, 220: 158~176.
- Zhang Zeming, Dong Xin, Liu Feng, Lin Yanhao, Yan Rong, Santosh M. 2012a. Tectonic evolution of the Amdo terrane, central Tibet: Petrochemistry and zircon U-Pb geochronology. The Journal of Geology, 120(4): 431~451.
- Zhang Zeming, Dong Xin, Liu Feng, Lin Yanhao, Yan Rong, He Zhenyu, Santosh M. 2012b. The making of Gondwana: Discovery of 650 Ma HP granulites from the North Lhasa, Tibet. Precambrian Research, 212: 107~116.
- Zhao Guochun, Wang Yuejun, Huang Baochun, Dong Yumpeng, Li Sanzhong, Zhang Guowei, Yu Shan. 2018. Geological reconstructions of the East Asian blocks: From the breakup of Rodinia to the assembly of Pangea. Earth-Science Reviews, 186: 262~286.
- Zhao Jianxin, McCulloch M T, Korsch R J. 1994. Characterisation of a plume-related ~800 Ma magmatic event and its implications for basin formation in central-southern Australia. Earth and Planetary Science Letters, 121(3-4): 349~367.
- Zhao Junhong, Zhou Meifu, Yan Danping, Zheng Jianping, Li Jianwei. 2011. Reappraisal of the ages of Neoproterozoic strata in South China: No connection with the Grenvillian orogeny. Geology, 39(4): 299~302.
- Zheng Yongfei, Wu Rongxin, Wu Yuanbao, Zhang Shaobing, Yuan Honglin, Wu Fuyuan. 2008a. Rift melting of juvenile arc-derived crust: Geochemical evidence from Neoproterozoic volcanic and granitic rocks in the Jiangnan Orogen, South China. Precambrian Research, 163(3-4): 351~383.
- Zheng Yongfei, Gong Bing, Zhao Zifu, Wu Yuanbao, Chen Fukun, 2008b. Zircon U-Pb age and O isotope evidence for Neoproterozoic low-¹⁸O magmatism during supercontinental rifting in South China: Implications for the snowball Earth event. American Journal of Science, 308(4): 484~516.
- Zhou Hongsheng, Ma Changqian, Zhang Chao, Chen Ling, Zhang Jinyang, Yu Zhenbing. 2008. Yanshanian aluminous A-type granitoids in the Chunshui of Biyang, south margin of North China Craton: Implications from petrology, geochronology and geochemistry. Acta Petrologica Sinica, 24 (1): 49~64 (in Chinese with English abstract).
- Zhou Meifu, Yan Damping, Kennedy A K, Li Yunqian, Ding Jun. 2002. SHRIMP U-Pb zircon geochronological and geochemical evidence for Neoproterozoic arc-magmatism along the western margin of the Yangtze Block, South China. Earth and Planetary Science Letters, 196(1-2): 51~67.
- Zhou Meifu, Ma Yuxiao, Yan Damping, Xia Xiaoping, Zhao Junhong, Sun Min. 2006. The Yanbian Terrane (Southern Sichuan Province, SW China): A Neoproterozoic arc assemblage in the western margin of the Yangtze Block. Precambrian Research, 144(1-2): 19~38.
- Zhou Xiang, Zheng Jianping, Li Yibing, Griffin W L, Xiong Qing, Moghadam H S, O'Reilly S Y. 2019. Neoproterozoic sedimentary rocks track the location of the Lhasa Block during the Rodinia breakup. Precambrian Research, 320: 63~77.
- Zhu Dichen, Chung Sunlin, Mo Xuanxue, Zhao Zhidan, Niu Yaoling, Song Biao, Yang Yueheng. 2009a. The 132 Ma Comei-Bunbury large igneous province: Remnants identified in present-day SE Tibet and SW Australia. Geology, 37(7): 583~586.
- Zhu Dichen, Mo Xuanxue, Niu Yaoling, Zhao Zhidan, Wang Liquan, Liu Yongsheng, Wu Fuyuan. 2009b. Geochemical investigation of early Cretaceous igneous rocks along an east-west traverse throughout the central Lhasa terrane, Tibet. Chemical Geology, 268(3-4): 298~312.
- Zhu Dichen, Mo Xuanxue, Zhao Zhidan, Niu Yaoling, Wang Liquan, Chu Qihong, Pan Guitang, Xu Jifeng, Zhou Changyong. 2010. Presence of Permian extension- and arc-type magmatism in southern Tibet: Paleogeographic implications. GSA Bulletin, 122(7-8): 979~993.
- Zhu Dichen, Zhao Zhidan, Niu Yaoling, Mo Xuanxue, Chung Sunlin, Hou Zengqian, Wang Liquan, Wu Fuyuan. 2011. The Lhasa Terrane: Record of a microcontinent and its histories of drift and growth. Earth and Planetary Science Letters, 301(1-2): 241~255.
- Zhu Dichen, Zhao Zhidan, Niu Yaoling, Dilek Y, Wang Qing, Ji Wenhua, Dong Guochen, Sui Qinglin, Liu Yongsheng, Yuan Honglin, Mo Xuanxue. 2012. Cambrian bimodal volcanism in the Lhasa Terrane, southern Tibet: Record of an early Paleozoic Andean-type magmatic arc in the Australian proto-Tethyan margin. Chemical Geology, 328: 290~308.
- Zhu Dichen, Zhao Zhidan, Niu Yaoling, Dilek Y, Hou Zengqian, Mo Xuanxue. 2013. The origin and pre-Cenozoic evolution of the Tibetan Plateau. Gondwana Research, 23(4): 1429~1454.

参 考 文 献

- 郭芳放,姜常义,苏春乾,夏明哲,夏昭德,魏巍. 2008. 准噶尔板块东南缘沙尔德兰地区A型花岗岩构造环境研究. 岩石学报, 24 (12): 2778~2788.
- 侯可军,李延河,田有荣. 2009. LA-MC-ICP-MS锆石微区原位U-Pb定年技术. 矿床地质, 28(4): 481~492.
- 胡道功,吴珍汉,江万,石玉若,叶培盛,刘琦胜. 2005. 西藏念青唐古拉岩群SHRIMP锆石U-Pb年龄和Nd同位素研究. 中国科学: 地球科学, 35(1): 29~37.
- 蒋少涌,赵葵东,姜耀辉,戴宝章. 2008. 十杭带湘南桂北段中生代A型花岗岩带成岩成矿特征及成因讨论. 高校地质学报, 14(4):

- 496~509.
- 李璞. 1955. 西藏东部地质的初步认识. 科学通报, (7): 62~71.
- 莫宣学, 董国臣, 赵志丹, 周肃, 王亮亮, 邱瑞照, 张风琴. 2005. 西藏冈底斯带花岗岩的时空分布特征及地壳生长演化信息. 高校地质学报, 11(3): 281~290.
- 潘桂棠, 莫宣学, 侯增谦, 朱弟成, 王立全, 李光明, 赵志丹, 耿全如, 廖忠礼. 2006. 冈底斯造山带的时空结构及演化. 岩石学报, 22(3): 521~533.
- 王明, 李才, 解超明, 吴彦旺, 苏犁, 胡培远. 2012. 聂荣微陆块花岗片麻岩锆石 LA-ICP-MS U-Pb 定年——新元古代基底岩石的发现及其意义. 岩石学报, 28(12): 4101~4108.
- 吴福元, 李献华, 郑永飞, 高山. 2007. Lu-Hf 同位素体系及其岩石学应用. 岩石学报, 23(2): 185~220.
- 吴元保, 郑永飞. 2004. 锆石成因矿物学研究及其对 U-Pb 年龄解释的制约. 科学通报, 49(16): 1589~1604.
- 解超明, 李才, 王明, 吴彦旺, 胡兆初. 2014. 藏北聂荣微陆块的构造亲缘性——来自 LA-ICP-MS 锆石 U-Pb 年龄及 Hf 同位素的制约. 地质通报, 33(11): 1778~1792.
- 周红升, 马昌前, 张超, 陈玲, 张金阳, 余振兵. 2008. 华北克拉通南缘泌阳春水燕山期铝质 A 型花岗岩类: 年代学、地球化学及其启示. 岩石学报, 24(1): 49~64.

Oceanic subduction along the northwestern margin of the Rodinia: Evidence from the Tonian granite gneisses in the Amdo area, northern Tibet

YANG Ning, HU Peiyuan*, ZHAI Qingguo, TANG Yue, LIU Yiming, LI Jinyong

Institute of Geology, Chinese Academy of Geological Sciences, Beijing 100037, China

* Corresponding author: azure_jlu@126.com

Abstract

The paleogeographic reconstruction of Rodinia supercontinent and the scheme of blocks have always been the focus and frontier of earth scientists at home and abroad. At present, the origin and paleogeographic location in the Rodinia supercontinent of the blocks in the Qinghai-Tibet Plateau are not clear. The comparative study of magmatic events is one of the effective methods to solve this problem. In this paper, LA-ICP-MS zircon U-Pb dating, petrogeochemistry, and zircon Hf and whole-rock Sr-Nd isotopic analyses of the granitic gneisses from the Amdo microcontinent in the central Tibetan Plateau are reported. The protoliths of these granitic gneisses were formed at 802~801 Ma, have heterogeneous zircon Hf and homogeneous whole Nd isotopic compositions ($\epsilon_{\text{Hf}}(t) = -9.4 \sim +1.9$; $\epsilon_{\text{Nd}}(t) = -4.8 \sim -3.4$) and ancient crustal model ages (2289~1575 Ma), and were probably generated by melting of mantle-modified Proterozoic crust and subsequent extensive crystallization differentiation. All samples have low P_2O_5 contents, that is negatively correlated with SiO_2 contents, and the samples contain a small amount of hornblende minerals, which is similar to those of I-type granite. Some rocks have high contents of high field strength elements ($Zr + Ce + Nb + Y > 350 \times 10^{-6}$) and zircon saturation temperature ($> 800^{\circ}\text{C}$) of A-type granite affinity. Finally, we propose that the granitic gneisses were probably formed in a back-arc basin environment, and could be compared with coeval magmatic rocks in Madagascar, Seychelles, and western India. This work provides new information for reconstruction of the Rodinia supercontinent.

Key words: Tibetan Plateau; Amdo; whole-rock geochemistry; zircon U-Pb dating